ACS Partner Journal

ENVIRONMENT & HEALTH

pubs.acs.org/EnvHealth

Article

Effect of Fluorine Atoms and Piperazine Rings on Biotoxicity of Norfloxacin Analogues: Combined Experimental and Theoretical Study

Chuanxi Yang,[#] Xiaoning Wang,[*,#] Xinyan Zhao, Yongkun Wu, Jingyan Lin, Yuhan Zhao, Yiyong Xu, Kaipeng Sun, Chao Zhang, Ziheng Wan, Weihua Zhao, Yihua Xiao, Haofen Sun, Dong Chen, Wenping Dong, Tieyu Wang, and Weiliang Wang[*]

Cite This: *Environ. Health* 2024, 2, 886−901

Read Online

ACCESS | Metrics & More | Article Recommendations | Supporting Information

ABSTRACT: To clarify the effect of the fluorine atom and piperazine ring on norfloxacin (NOR), NOR degradation products (NOR-DPs, P1−P8) were generated via UV combined with hydrogen peroxide (UV/H_2O_2) technology. NOR degradation did not significantly affect cytotoxicity of NOR against BV2, A549, HepG2, and Vero E6 cells. Compared with that of NOR, mutagenicity and median lethal concentration of P1−P8 in fathead minnow were increased, and bioaccumulation factor and oral median lethal dose of P1−P8 in rats were decreased. Molecular docking was used to evaluate the inhibitory effect of DNA gyrase A (gyrA) on NOR-DPs to determine the molecular-level mechanism and establish the structure−activity relationship. Results indicated that the most common amino acid residues were Ile13, Ser27, Val28, Gly31, Asp36, Arg46, Arg47, Asp157, and Gly340; hydrogen bonds and hydrophobic interactions played key roles in the inhibitory effect. Binding area (BA) decreased from 350.80 Å^2 (NOR) to 346.21 Å^2 (P1), and the absolute value of binding energy (|BE|) changed from 2.53 kcal/mol (NOR) to 2.54 kcal/mol (P1), indicating that the fluorine atom mainly affects BA. The piperazine ring clearly influenced BA and |BE|. "Yang ChuanXi Rules" were used to explain effects of molecular weight (MW), BA, |BE|, and sum of $\eta_1 + \eta_2$ (η_1: normalization of BA, η_2: normalization of |BE|) and predict biotoxicity of NOR-DPs based on half-maximum inhibitory concentration (IC_{50}), half-minimal inhibitory concentration (MIC_{50}), and half-minimal bactericidal concentration (MBC_{50}) values.

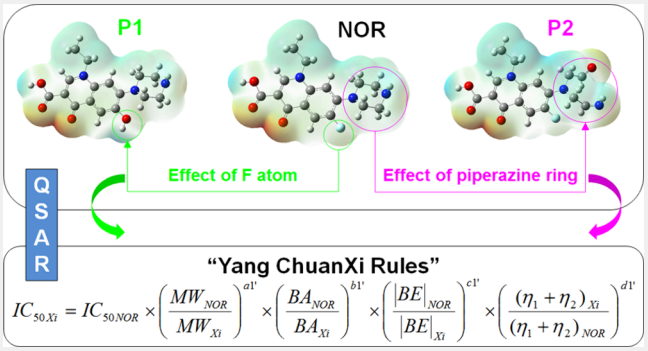

KEYWORDS: *norfloxacin, biotoxicity, inhibition effect, molecular docking, structure−activity relationship*

1. INTRODUCTION

Emerging contaminants (ECs) are newly discovered or concerning pollutants that pose risks to the ecological environment or human health; existing measures do not address these contaminants and thus cannot effectively prevent and manage ECs. Recently, ECs have attracted general attention, as they include persistent organic pollutants (POPs), endocrine disrupters, microplastics, and antibiotics.[1,2] Biotoxic, bioaccumulating, persistent antibiotics have attracted widespread attention and are discharged into the water environment through runoff and other methods.[3] Fluoroquinolone (FQ) antibiotic norfloxacin (NOR) is commonly and widely used to treat intestinal, urinary tract, and respiratory system infections as an anti-infective drug and mainly targets Gram-positive bacteria or staphylococcus.[4] NORs are found profusely in the water environment of China, with concentrations of 21.1 ng/L in Yellow Sea,[5] 62.5−136 ng/L in Pearl River,[6] 572 ng/L in Laizhou Bay,[7] 28.8 ng/L in Weihe River,[8] and 136−1620 ng/L in wastewater from Chongqing Hospital.[9] NORs are characterized by environmental persistence and bioaccumulation; even at low concentrations in water environment, NORs may cause significant environmental effects and health risks, and their hazards are latent and concealed.[10] Removal of NOR from aqueous solutions has been extensively researched by physical, chemical, and biological methods.[3,11] Taking into consideration the removal rate, economical efficiency, and environmental risk, UV combined with hydrogen peroxide (UV/H_2O_2) uses the strong oxidizing agent H_2O_2 in the degradation of NOR, forming mainly CO_2

Received: May 22, 2024
Revised: August 13, 2024
Accepted: August 14, 2024
Published: August 22, 2024

https://doi.org/10.1021/envhealth.4c00095
Environ. Health 2024, 2, 886−901

and water. Furthermore, NOR has been demonstrated to cause embryonic loss in monkeys when administered at doses 10 times the maximal human dose.[11,12]

NOR inhibits bacterial DNA gyrase to prevent DNA replication and transcription from progressing.[13] DNA gyrase is topoisomerase II that can be used to convert DNA plasmids (pBR322) from flabby to supercoiled configuration and change the topological structure of DNA.[14] In addition, DNA gyrase can facilitate separation of diploid DNA at a late stage of DNA replication, preserve long DNA strands in fine cytoplasm, and establish a high-level DNA structure for efficient DNA duplication.[15] DNA gyrase is ATP hydrolase in prokaryotes with heterotetrameric enzyme structure $(gyrA)_2(gyrB)_2$ that is composed of two kinds of subunits; this enzyme was discovered in *Escherichia coli* (*E. coli*) in 1976 and plays a very important role in DNA replication, transcription, and chromosome segregation.[16,17] In *E. coli*, DNA gyrase is composed of tetramers with two molecular subunits of gyrA (97 kDa) and two molecular subunits of gyrB (90 kDa) that act at a single position. DNA gyrase is unique to prokaryotes, such as bacteria. This gene is not present in eukaryotic cells, such as those of higher animals and plants, and thus acts as an ideal drug-target and target for anticancer drugs and antibiotics.[18,19] Subunit A participates in the binding and inhibition of FQs, which are composed of two domains. The N-terminal breakage-reunion domain is the first domain and is also known as the G segment at the DNA gate. Its function involves binding, cleaving, and resealing the DNA segment and accessing the C-terminal domain (CTD) as the second domain. In this enzyme, three protein−protein interfaces form gates (central DNA gates) that can open and close, allowing DNA to pass through the enzyme. The GyrA subunit consists of the following domains: winged-helix domain (WHD), which contains catalytic tyrosine residue; long domain, classified as coiled-coil; tower domain; and variable C-terminus.[20] Therefore, clarifying the inhibitory effect of NOR degradation products (NOR-DPs) on gyrA is important for managing risks and controlling NOR and other ECs.

However, shortcomings refer to traditional experimental methods (east two-hybrid, dual luciferase reporter system, animal *in vivo* experiments) used for evaluating biotoxicity of ECs, including long experimental cycles, complicated operations, expensive equipment, poor experimental repeatability, and low sensitivity. Computational simulations are widely used because of their high efficiency, high accuracy, and low cost; thus, these simulations are highly important for toxicology explorations and evaluating environmental effects of NOR and other chemicals.[21] Pillai et al. discussed use of computational simulation to predict pharmacokinetics and rank drug candidates to achieve appropriate exposures; results provided important insights into safety and efficacy.[22] Govender et al. proposed a computational simulation model to clarify the mechanism used by DNA substrates; in this process, gyrase captures contiguous DNA segments with high probability, irrespective of the superhelix density of the DNA substrate, setting up equilibrium for transported segments across the DNA gate.[23] Hence, computational simulation technology is a popular approach for evaluating biotoxicology and environmental effects of organic pollutants because technology is rapid, accurate, and effective. However, the results of biotoxicity with only computational simulations display high randomicity due to the lack of a real environment. Hence, it is significant and meaningful to establish a biotoxicity evaluation method combining theory and experiment.

In this study, NOR-DPs/NOR degradation solution (NOR-DS) was obtained via UV/H_2O_2 degradation, and products were analyzed via a liquid chromatography−mass spectrometry (LC-Q-TOF-MS) system. Viability and cytotoxic effects of NOR/NOR-DS on mouse microglial BV2 cells, human lung type II epithelial A549 cells, human hepatocellular carcinoma HepG2 cells, and monkey kidney epithelial Vero E6 cells were examined, and effects were detected via a cell counting kit-8 (CCK-8) and cytotoxicity lactate dehydrogenase (LDH). A toxicity estimation software tool (T.E.S.T.) was used to calculate several biotoxicity parameters, including developmental toxicity, mutagenicity, bioaccumulation factor, median lethal concentration (LC_{50}) of NOR/NOR-DS to fathead minnow in 96 h, median immune glucose concentration (IGC_{50}) of NOR/NOR-DS to *Tetrahymena pyriformis* after 48 h, LC_{50} of NOR/NOR-DS to *Daphnia magna* after 48 h, and median lethal dose (LD_{50}) of orally administered NOR/NOR-DPs to rats. Combination parameters of pocket, binding mode, binding area (BA), and absolute value of binding energy (|BE|) for NOR/NOR-DPs and gyrA were determined via Autodock software. The equation "Yang ChuanXi Rules (YCX-Rules)" was proposed for predicting biotoxicity of NOR/NOR-DPs. Yang ChuanXi Rules were used to explain effects of molecular weight (MW), BA, |BE|, and sum of $\eta_1 + \eta_2$ (η_1: normalization of BA, η_2: normalization of |BE|) and predict biotoxicity of NOR-DPs based on half-maximum inhibitory concentration (IC_{50}), half-minimal inhibitory concentration (MIC_{50}), and half-minimal bactericidal concentration (MBC_{50}) values. The YCX-Rules equation was proposed to predict biotoxicity of compounds and degradation products. Combined experimental cellular damage and theoretical study of computational toxicology integrated empirical data with computational models to gain comprehensive insights. In this study, we emphasize the unique insights gained from the combined experimental and theoretical approach to understanding the biotoxicity of NOR and NOR-DPs. Results provide theoretical support for toxicity, health effects, risk management, and control of EC degradation products in aquatic environments.

2. MATERIALS AND METHODS

2.1. Chemicals

NOR was purchased from Shanghai Macklin Biochemical Co., Ltd. (Shanghai, China). Hydrogen peroxide (H_2O_2, 30%), formic acid (HCOOH), and acetonitrile (CH_3CN) are described in detail in Supplementary Text S1.1. A CCK-8 kit and a LDH assay kit-WST were acquired from Dojindo Laboratories (Kumamoto, Japan).

2.2. Preparation and Detection of NOR-DPs

The NOR degradation process and NOR-DPs structures were determined in our previous research.[24] Details are described in Supplementary Text S1.2.

2.3. Detection of Cell Toxicity Induced by NOR/NOR-DS

2.3.1. *In Vitro* Cell Line Culture and Treatments. BV2, A549, HepG2, and Vero E6 cells were cultured in Dulbecco's Modified Eagle Medium (DMEM, Gibco); McCoy's 5A Media (modified with Tricine, Gibco); Minimum Essential Medium Eagles with Earle's Balanced Salts (MEM-EBSS); and 1% nonessential amino acids (NEAA, Gibco) and DMEM supplemented with 10% fetal bovine serum (FBS, Gibco), respectively.[25−28] Details are described in Supplementary Text S1.3.

https://doi.org/10.1021/envhealth.4c00095
Environ. Health 2024, 2, 886−901

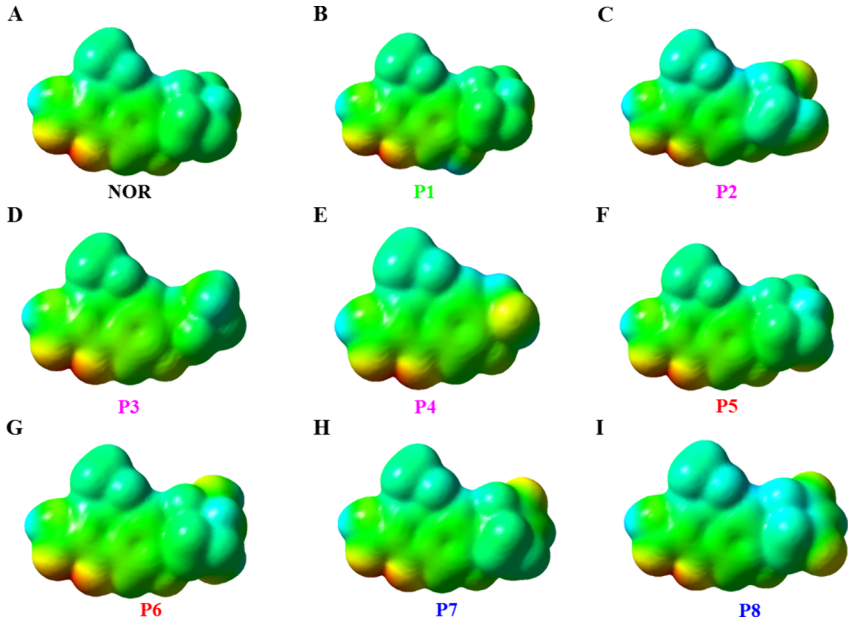

Figure 1. ESP of (a) NOR, (b) P1, (c) P2, (d) P3, (e) P4, (f) P5, (g) P6, (h) P7, and (i) P8.

2.3.2. Cell Viability Assay. Cell viability of BV2, A549, HepG2, and Vero E6 cells after exposure to NOR/NOR-DS was determined by a CCK-8 kit.[29] Details are described in Supplementary Text S1.4.

2.3.3. Cytotoxicity Assay. Cytotoxicity of BV2, A549, HepG2, and Vero E6 cells after exposure to NOR/NOR-DS was determined by an LDH kit.[30] Details are described in Supplementary Text S1.5.

2.4. Calculation of Biotoxicity

The toxicity of NOR-DPs during the NOR degradation process must be considered. The following theoretical values were calculated: developmental toxicity, mutagenicity, bioaccumulation factor, concentration of compounds that cause 50% death of fathead minnows after 96 h (fathead minnow LC_{50} in 96 h, mg/L), concentration of compounds that cause 50% immune glucose concentration in *Tetrahymena pyriformis* after 48 h (*T. pyriformis* IGC_{50} in 48 h, mg/L), concentration of compounds that cause 50% death in *Daphnia magna* after 48 h (*D. magna* LC_{50} in 48 h, mg/L), and concentration of compounds that cause 50% death in oral rats (oral rat LD_{50}, mg/kg); these values were measured for NOR and NOR-DPs (P1, P2, P3, P4, P5, P6, P7, and P8) and were assessed by T.E.S.T. software based on an quantitative structure−activity relationship (QSAR) model.[31] T.E.S.T. software was opened, and then "File" and "import from MDL modifier" were clicked. Compounds were saved in mol format. Parameters used were developmental toxicity, mutagenicity, bioaccumulation factor, fathead minnow LC_{50} after 96 h (mg/L), *T. pyriformis* IGC_{50} after 48 h (mg/L), *D. magna* LC_{50} after 48 h (mg/L), and oral rat LD_{50} (mg/kg); subsequently, "predicted value" was defined as obtained values. Finally, Origin software was used to determine optimal values, and each parameter was plotted as an ordinate.

2.5. Molecular Docking

The macromolecular structure of gyrA used for molecular docking simulation was obtained from the Protein Data Bank (PDB ID 2Y3P; https://www.rcsb.org), after which undesired structures were minimized and managed by AutoDock (version 4.2).[13,24,32] The AutoGrid 4.2 default parameter was used in AutoGrid4 to construct an affinity map of each atom, desolvation map, and electrostatic map. Maximum allowable initial energy was 0. Maximum number of retries was 10 000. Translation time was 0.2 Å for each step. The order of quaternion and torsion was 5° for each step.[33] Macromolecules and small molecules were screened for improved interaction performance.[34−36] Details are described in Supplementary Text S1.6.

2.6. Compound Data Processing

The initial data of BA and |BE| for NOR, P1, P2, P3, P4, P5, P6, P7, and P8 binding to gyrA were processed. Details are described in Supplementary Text S1.7.

2.7. Statistical Analysis

The experimental data are expressed as the standard error of the mean (SEM). GraphPad Prism version 6.0 was used for data analysis. One-way analysis of variance for multiple comparisons was used to analyze differences between groups, and $P < 0.05$ was considered to indicate statistical significance.

3. RESULTS

3.1. Pathway and Structures of NOR-DPs

NOR-DPs were acquired through UV/H_2O_2 degradation technology and analyzed via a LC-Q-TOF-MS system.[24] Degradation product structure and degradation pathway are shown in Figure S1 and Table S1. In pathway 1, the fluorine atom was replaced directly by a hydroxide radical, and a hydrolated-NOR intermediate formed as P1 (F → ·OH, m/z = 317.34). In pathway 2, P2 (+O−2H, m/z = 333.31) was acquired after the piperazine ring of NOR was cleaved, one of the nitrogens for the piperazine ring was exposed, and a carbonyl was added. In pathway 3, loss of C_2H in NOR led to cleavage of the piperazine ring P3 (−2C−H, m/z = 293.29), exposing nitrogen in the piperazine ring; in pathway 3, with continuous piperazine ring clavation and ·OH oxidation, P4 (−4C−N−6H+O, m/z = 266.23) was acquired by a cracked site for the piperazine ring of P3, nitrogen for the piperazine ring was exposed, and a hydroxyl group was added for P4. In pathway 4, P5 (+OH, m/z = 335.33) was acquired through hydroxylation of the piperazine ring of NOR, and one hydroxyl group was added for P5. In pathway 4, with continuous ·OH oxidation, P6 (+2O2H, m/z = 351.33) was acquired by hydroxylation of the piperazine ring of P5, and two hydroxyl groups were added to P6. In pathway 5, P7 (+O−2H, m/z = 333.31) was acquired through carbonylation of the piperazine ring of NOR, and one carbonyl group was added for P7. In pathway 5, with continuous hydroxylation, P8 (+2O−4H, m/z = 347.30) was acquired by carbonylation of the piperazine ring

https://doi.org/10.1021/envhealth.4c00095
Environ. Health 2024, 2, 886−901

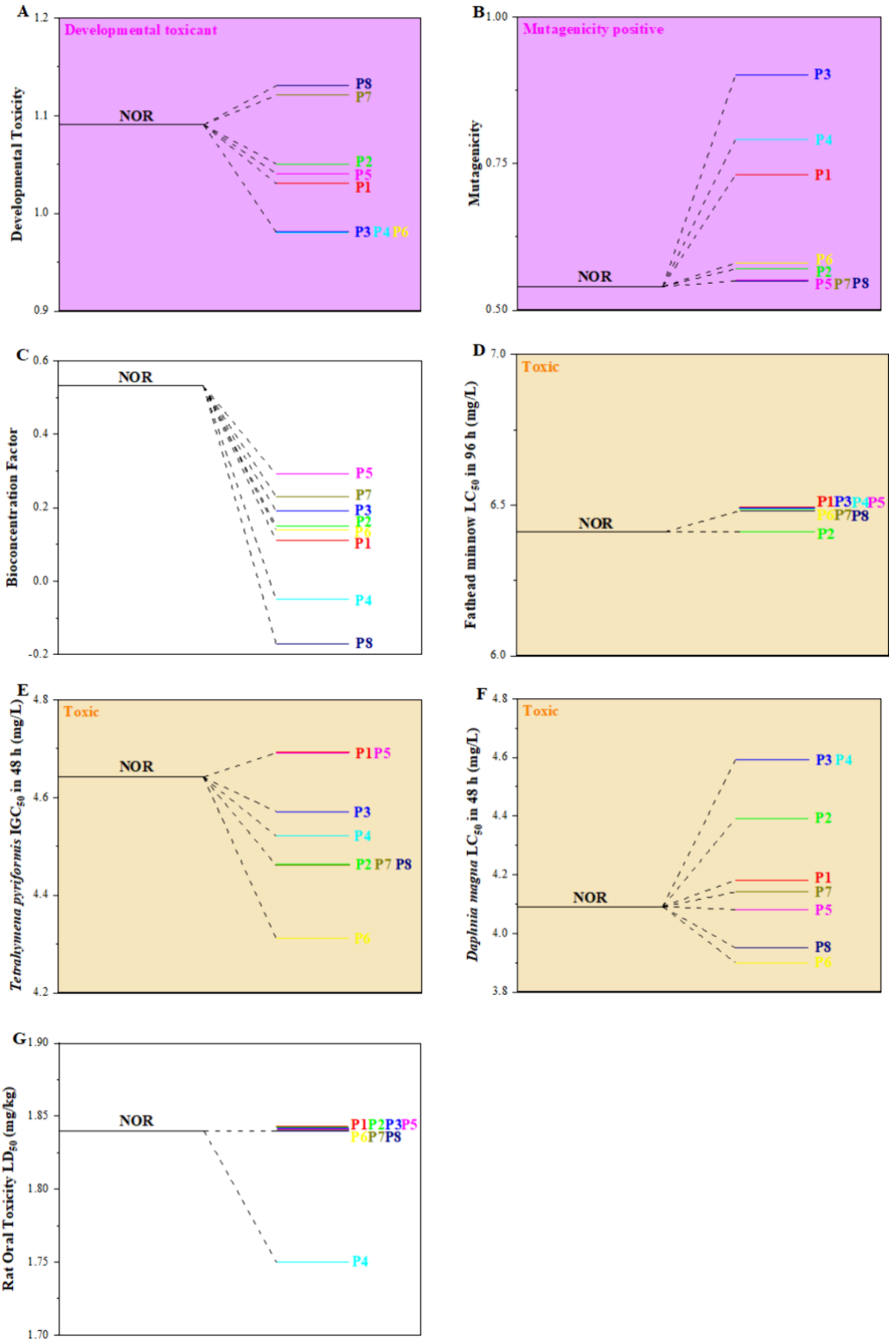

Figure 2. Theories of (a) developmental toxicity, (b) mutagenicity, (c) bioaccumulation factor, (d) fathead minnow LC_{50} after 96 h (mg/L), (e) *T. pyriformis* IGC_{50} after 48 h (mg/L), (f) *D. magna* LC_{50} after 48 h (mg/L), and (g) oral rat LD_{50} (mg/kg) for NOR and NOR-DPs.

of P7, and two carbonyl groups were added for P8. In brief, the fluorine-substituted product of P1 (F → ·OH), piperazine ring-cleaved products of P2 (+O−2H), P3, and P4 (−2C−H and −4C−N-6H+O, respectively), hydroxylated products of P5 and P6 (+OH and +2O2H, respectively), and carbonylated products of P7 and P8 (+O−2H and +2O−4H, respectively) of NOR via UV/H_2O_2 degradation reaction were analyzed via the LC-Q-TOF-MS system. Details are described in Supplementary Text S2. The electrostatic potential (ESP) of NOR in Figure 1 and Figure S2 shows that fluorine atoms and piperazine rings are negative values with low electron cloud density, which means the fluorine atoms and piperazine rings were vulnerable to attack to generate P1−P8. Therefore, the degradation products and their degradation pathways of NOR

https://doi.org/10.1021/envhealth.4c00095
Environ. Health 2024, 2, 886−901

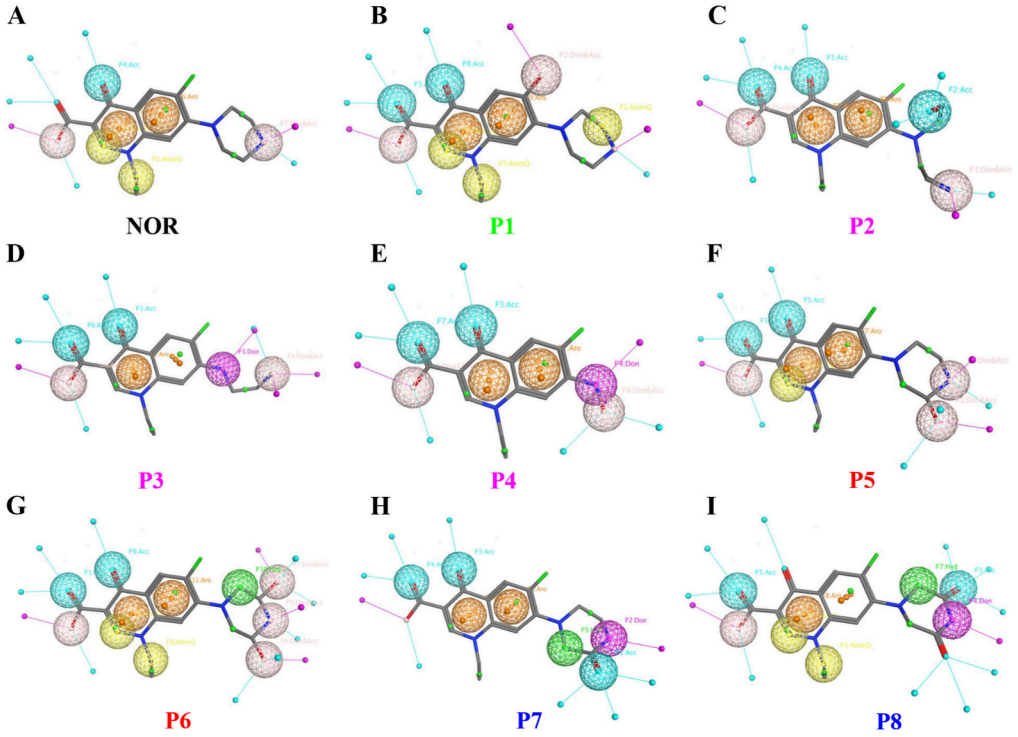

Figure 3. Key functional-effector groups and structural-effector pharmacophores for (a) NOR, (b) P1, (c) P2, (d) P3, (e) P4, (f) P5, (g) P6, (h) P7, and (i) P8, which combined with gyrA.

by UV/H_2O_2 were reasonable based experimental and theoretical study.

3.2. NOR/NOR-DS Induced Cellular Damage

3.2.1. Cell Viability for Cells Treated with NOR/NOR-DS. To determine cytotoxic effects of NOR and NOR-DS on BV2, A549, HepG2, and Vero E6 cells, cell viability was evaluated via a CCK-8 kit after treatment with different percentages of NOR or NOR-DS (0.04%, 0.08%, 0.16%, 0.31%, 0.63%, 1.25%, 2.50%, 5.00%, or 10.00% of 20 mg/L NOR solution before or after 180 min UV/H_2O_2 degradation) for 24 h. Results showed that NOR/NOR-DS exhibited an inconspicuous toxic effect on BV2, A549, HepG2, and Vero E6 cells; viability of BV2 was decreased by 0.16% NOR/NOR-DS without significant changes (Figure S3A, Figure S4A−B, Table S2, and Table S3); viability of A549 (Figure S3B, Figure S4C−D, Table S2, and Table S3) and HepG2 (Figure S3C, Figure S4E−F, Table S2, and Table S3) was decreased by 10.00% NOR/NOR-DS without significant changes; and viability of Vero E6 was decreased by 2.50% and 10.00% NOR/NOR-DS without significant changes (Figure S3D, Figure S4G−H, Table S2, and Table S3). Details are described in Supplementary Text S3.

3.2.2. Cytotoxicity in Cells Treated with NOR/NOR-DS. To determine cytotoxic effects of NOR and NOR-DS on BV2, A549, HepG2, and Vero E6 cells, cytotoxicity was evaluated by an LDH kit after treatment with different percentages of NOR or NOR-DS (0.04%, 0.08%, 0.16%, 0.31%, 0.63%, 1.25%, 2.50%, 5.00%, or 10.00% of 20 mg/L NOR solution before or after 180 min UV/H_2O_2 degradation) for 24 h. Compared with the 0.00% NOR group, the NOR group did not exhibit significantly different cytotoxicity against BV2, A549, HepG2, and Vero E6 cells (Figure S5, Figure S6, and Table S4). Compared with the 0.00% NOR-DS treatment group, the NOR-DS treatment group did not exhibit significantly different cytotoxicity against BV2, A549, HepG2, and Vero E6 cells (Figure S5, Figure S6, and Table S5). Results showed that NOR and NOR-DS had inconspicuous toxic effects on BV2, A549, HepG2, and Vero E6 cells. Details are described in Supplementary Text S4.

3.3. Calculation for Biotoxicity of NOR/NOR-DPs

The simulated biotoxicity for degradation products is a significant indicator of catalysts or degradation process.[37] To evaluate safety of the UV/H_2O_2 process for NOR degradation, developmental toxicity, mutagenicity, bioaccumulation factor, fathead minnow LC_{50} after 96 h (mg/L), *T. pyriformis* IGC_{50} after 48 h (mg/L), *D. magna* LC_{50} after 48 h (mg/L), and oral rat LD_{50} (mg/kg) were estimated with NOR and NOR-DPs (P1, P2, P3, P4, P5, P6, P7, and P8) by T.E.S.T. Here, intermediates of NOR-DPs generated from changing fluorine atoms to hydroxide radicals (P1), cleaving piperazine rings (P2, P3, P4), hydroxylating piperazine rings (P5, P6), and adding carbonyl to piperazine rings (P7, P8) were chosen as final products to assess biotoxicity of the solution after treatment with the UV/H_2O_2 degradation process.

NOR and NOR-DPs exhibited a "developmental toxicant" phenotype, while UV/H_2O_2 treatment decreased the developmental toxicity of P1, P2, P3, P4, P5, and P6 and heightened the developmental toxicity of P7 and P8 (Figure 2A and Table S6). NOR and NOR-DPs exhibited "mutagenicity positive" status, while UV/H_2O_2 treatment heightened mutagenicity of P1, P2, P3, P4, P5, P6, P7, and P8 (Figure 2B and Table S6). The UV/H_2O_2 process decreased the bioaccumulation factor of P1, P2, P3, P4, P5, P6, P7, and P8 (Figure 2C and Table S6). NOR and NOR-DPs exhibited a "toxic" phenotype, while UV/H_2O_2 treatment led to equivalent fathead minnow LC_{50} at 96 h in P2 and heightened fathead minnow LC_{50} at 96 h in P1, P3, P4, P5, P6, P7, and P8 (Figure 2D and Table S6). NOR and NOR-DPs exhibited a toxic phenotype, while UV/H_2O_2

https://doi.org/10.1021/envhealth.4c00095
Environ. Health 2024, 2, 886−901

treatment decreased activity of *T. pyriformis* IGC_{50} after 48 h in P2, P3, P4, P6, P7, and P8 and increased activity of *T. pyriformis* IGC_{50} after 48 h in P1 and P5 (Figure 2E and Table S6). NOR and NOR-DPs exhibited a toxic phenotype, while UV/H_2O_2 treatment decreased LC50 of P5, P6, and P8 and heightened LC_{50} of P1, P2, P3, P4, and P7 in *D. magna* after 48 h (Figure 2F and Table S6). UV/H_2O_2 treatment decreased the oral LD_{50} of P4 rats and generated equivalent values to the oral LD_{50} values of P1, P2, P3, P5, P6, P7, and P8 to rats (Figure 2G and Table S6). Details are described in Supplementary Text S5.

3.4. Combination of NOR/NOR-DPs and GyrA

3.4.1. Amino Acid Sequence of GyrA. The original sequence of amino acids in chain B of gyrA protein was consistent with the corresponding sequence on the National Center for Biotechnology Information (NCBI) Web site (Figure S7).

3.4.2. Interaction between NOR/NOR-DPs and GyrA. The key interaction pocket of gyrA with NOR/NOR-DPs is shown in Figures S8−S12; residues and interactions between NOR/NOR-DPs and gyrA are three-dimensional and two-dimensional and were determined by molecular docking simulation (Figures S13−S15, Figures S16−S18, Figures S19−S21, Figures S22−S24, and Figures S25−S27). Key combination processes of NOR/NOR-DPs and gyrA include hydrogen bonding and hydrophobic interactions (Table S7). Details are described in Supplementary Text S6.1−S6.5.

3.5. Structure−Activity Relationships of NOR/NOR-DPs and GyrA Complex

3.5.1. Analysis of the Structure of NOR/NOR-DPs. Functional groups in NOR and NOR-DPs included fluorine, carboxyl, carbonyl, benzene ring, heterocyclic carbon and nitrogen, hydrocarbon chain, piperazine ring, hydroxyl, and nitrogen groups (Figure S28A−I and Table S8). Details are described in Supplementary Text S7.

The key functional effector groups of NOR and NOR-DPs included carboxyl, carbonyl, and benzene rings and heterocyclic carbon and nitrogen compounds and involved hydrocarbon chains, piperazine rings, hydroxyl groups, and nitrogen (Figure 3A−I and Table S9). Key functional-effector groups of NOR combined with gyrA included carboxyl, carbonyl, benzene ring, carbon and nitrogen heterocycles, and hydrocarbon chain and piperazine ring groups (Figure 3A and Table S9) as well as structural-effector pharmacophores, including H-bond donor and H-bond acceptor (Don & Acc), Acc, aromatic center (Aro), Aro and defined qualified feature of atom (AtomQ), AtomQ, and Don & Acc (Figure 3A), respectively; key functional-effector groups of P1 combined with gyrA included carboxyl, carbonyl, benzene ring, carbon and nitrogen heterocycles, hydrocarbon chain, piperazine ring, and hydroxyl groups (Figure 3B and Table S9) as well as structural-effector pharmacophores, including Don & Acc and Acc, Acc, Aro, Aro and AtomQ, AtomQ, AtomQ, and Don & Acc (Figure 3B), respectively; key functional-effector groups of P2 combined with gyrA included carboxyl, carbonyl, benzene ring, carbon and nitrogen heterocycles, and nitrogen groups (Figure 3C and Table S9) as well as structural-effector pharmacophores, including Don & Acc and Acc, Acc, Aro, Aro, and Don & Acc (Figure 3C), respectively; key functional-effector groups of P3 combined with gyrA included carboxyl, carbonyl, heterocyclic of carbon and nitrogen, nitrogen (Figure 3D and Table S9), structural-effector pharmacophores, including Don & Acc and Acc, Acc, Aro, Don & Acc, and Don (Figure 3D), respectively; key functional-effector groups of P4 combined with gyrA included carboxyl, carbonyl, benzene ring, carbon and nitrogen heterocycles, hydroxyl and nitrogen groups (Figure 3E and Table S9) as well as structural-effector pharmacophores, including Don & Acc and Acc, Acc, Aro, Aro, Don, and Don & Acc (Figure 3E), respectively; key functional-effector groups of P5 combined with gyrA included carboxyl, carbonyl, benzene ring, carbon and nitrogen heterocycles, piperazine ring and hydroxyl groups (Figure 3F and Table S9) as well as structural-effector pharmacophores, including Don & Acc and Acc, Acc, Aro, Aro and AtomQ, Don & Acc, and Don & Acc (Figure 3F), respectively; key functional-effector groups of P6 combined with gyrA included carboxyl, carbonyl, benzene ring, carbon and nitrogen heterocycles, hydrocarbon chain, piperazine ring and hydroxyl groups (Figure 3G and Table S9) as well as structural-effector pharmacophores, including Don & Acc and Acc, Acc, Aro, Aro and AtomQ, AtomQ, Don & Acc and Hydrophobic centroid (Hyd), and Don & Acc (Figure 3G), respectively; key functional-effector groups of P7 combined with gyrA included carboxyl, carbonyl, benzene ring, carbon and nitrogen heterocycles, and piperazine ring groups (Figure 3H and Table S9) as well as structural-effector pharmacophores, including Acc, Acc, Aro, Aro, Don and Hyd (Figure 3H), respectively; key functional-effector groups of P8 combined with gyrA included carboxyl, carbonyl, carbon and nitrogen heterocycles, hydrocarbon chain and piperazine ring groups (Figure 3I and Table S9) as well as structural-effector pharmacophores, including Don & Acc and Acc, Acc, Aro and AtomQ, AtomQ, Don and Hyd (Figure 3I), respectively. Key functional effector groups common to NOR and NOR-DPs included carboxyl, carbonyl, carbon, and nitrogen heterocycle groups; key functional effector groups common to NOR and NOR-DPs included benzene rings, hydrocarbon chains, piperazine rings, hydroxyl rings, and nitrogen rings (Figure 3A−I and Table S9). Accordingly, common structural effector pharmacophores of NOR and NOR-DPs included Acc, Aro, and various structural effector pharmacophores of NOR and NOR-DPs, including Don, Hyd, and AtomQ (Figure 3A−I and Table S9).

van der Waals (VDW) forces were mapped on the molecular surface within 4.5 Å of NOR/NOR-DPs to illustrate hydrogen bonds and hydrophobic interactions. Hydrogen bonds formed by NOR/NOR-DPs involved carboxyl, carbonyl, piperazine ring, hydroxyl, and nitrogen groups whereas hydrophobic interactions involved benzene ring, carbon and nitrogen heterocycle, hydrocarbon chain, and piperazine ring (Figure S29A−I and Table S10). Hydrogen bonds formed for NOR involved carboxyl, carbonyl, and piperazine ring group whereas hydrophobic interactions involved benzene ring, carbon and nitrogen heterocycle, hydrocarbon chain, and piperazine ring (Figure S29A and Table S10); hydrogen bonds formed in P1 involved carboxyl, carbonyl, piperazine ring, and hydroxyl, and hydrophobic interaction involved benzene ring, carbon and nitrogen heterocycle, hydrocarbon chain, and piperazine ring (Figure S29B and Table S10); hydrogen bonds formed in P2 involved carboxyl, carbonyl, and nitrogen compounds, and hydrophobic interaction involved benzene ring and carbon and nitrogen heterocycle (Figure S29C and Table S10); hydrogen bonds in P3 involved carboxyl, carbonyl, and nitrogen groups, and hydrophobic interaction involved carbon and nitrogen heterocycle (Figure S29D and Table S10); hydrogen bonds in P4 involved carboxyl, carbonyl, hydroxyl, and nitrogen groups,

https://doi.org/10.1021/envhealth.4c00095
Environ. Health 2024, 2, 886−901

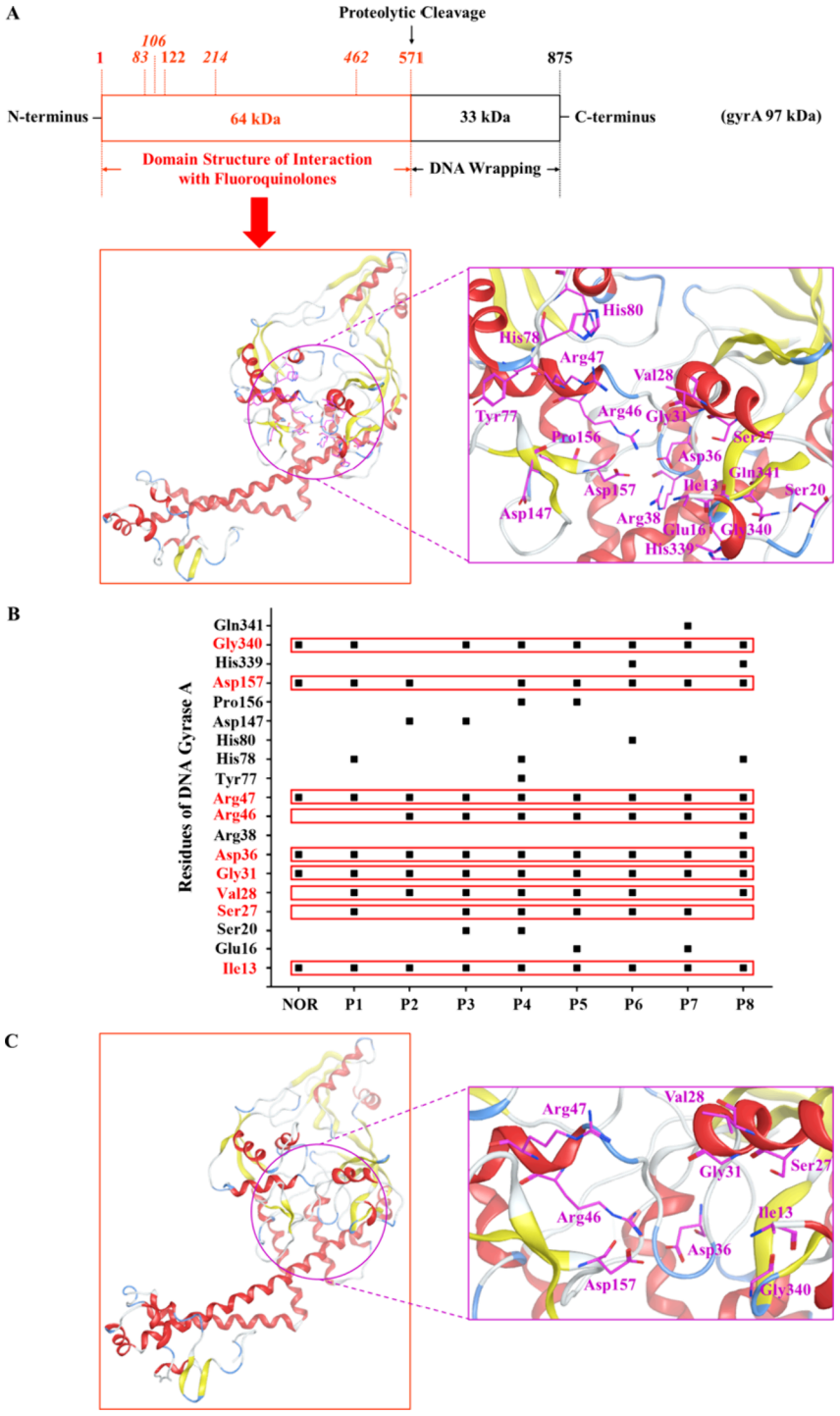

Figure 4. Domain structure of gyrA in *E. coli* and amino acids in the active pocket of gyrA that participate in NOR/NOR-DPS and gyrA combination (a); arrows indicate domain boundaries, and numbers indicate amino acid residues. The schematic diagram of the gyrA structure was adapted from Hashimi (2019).[38] Amino acids and residues with high frequency (≥6) participate in NOR/NOR-DPS and gyrA combination; amino acids with high frequency are labeled in red (b). X-ray diffraction structure and amino acids in the active pocket with high frequency of gyrA (c).

and hydrophobic interaction involved benzene ring and carbon and nitrogen heterocycle (Figure S29E and Table S10); hydrogen bonds in P5 involved carboxyl, carbonyl, piperazine ring, and hydroxyl groups, and hydrophobic interaction involved benzene ring, carbon and nitrogen heterocycle, and piperazine ring (Figure S29F and Table S10); hydrogen bonds in P6 involved carboxyl, carbonyl, piperazine ring, and hydroxyl groups, and hydrophobic interaction involved benzene ring, carbon and nitrogen heterocycle, hydrocarbon chain, and piperazine ring (Figure S29G and Table S10); hydrogen bonds in P7 involved carboxyl, carbonyl, and piperazine ring, and hydrophobic interaction involved benzene ring, carbon and nitrogen heterocycle, and piperazine ring (Figure S29H and Table S10); hydrogen bonds in P8 involved carboxyl, carbonyl, and piperazine ring, and hydrophobic interaction involved carbon and nitrogen heterocycle, hydro-

https://doi.org/10.1021/envhealth.4c00095
Environ. Health 2024, 2, 886−901

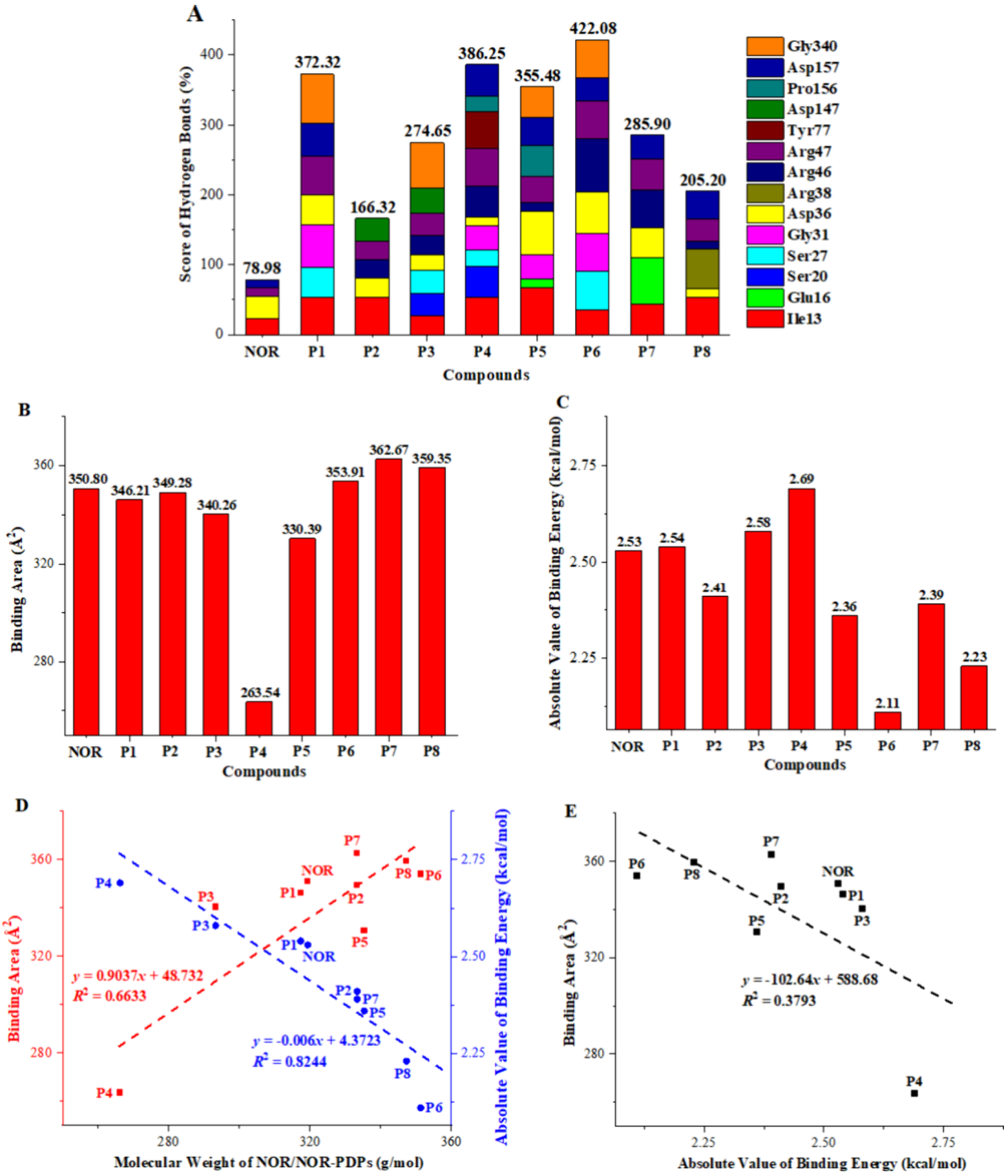

Figure 5. Values of hydrogen bonds (a), binding area (b), absolute value of binding energy (c), molecular weight, binding area, and absolute value of binding energy (d), and binding area and absolute value of binding energy (e) for NOR/NOR-DPs and gyrA.

carbon chain, and piperazine ring (Figure S29I and Table S10). Hydrogen bonds in NOR/NOR-DPs combined with gyrA commonly involved carboxyl and carbonyl, and various hydrogen bonds in NOR/NOR-DPs involved piperazine ring, hydroxyl, and nitrogen. Hydrophobic interactions in NOR/NOR-DPs combined with gyrA commonly involved heterocyclic carbon and nitrogen; various hydrophobic interactions in NOR/NOR-DPs involved benzene rings, hydrocarbon chains, and piperazine rings (Figure S29A–I and Table S10).

The potential reaction capacities of NOR/NOR-DPs and H_2O are shown in Figure S29J–R, and compounds that participate in hydrophobic interactions are presented as gaps for NOR/NOR-DPs containing hydrocarbon chains and piperazine rings. Hydrophobic interactions in NOR involved hydrocarbon chains and piperazine rings (Figure S29J); hydrophobic interactions in P1 involved hydrocarbon chains and piperazine rings (Figure S29K); hydrophobic interactions in P2 involved hydrocarbon chains (Figure S29L); hydro-

https://doi.org/10.1021/envhealth.4c00095
Environ. Health 2024, 2, 886–901

phobic interactions in P3 involved hydrocarbon chains and cleavable piperazine rings (Figure S29M); hydrophobic interactions in P4 involved hydrocarbon chains (Figure S29N); hydrophobic interactions in P5 involved hydrocarbon chains and piperazine rings (Figure S29O); hydrophobic interactions in P6 involved hydrocarbon chains (Figure S29P); hydrophobic interactions in P7 involved hydrocarbon chains and piperazine rings (Figure S29Q); hydrophobic interactions in P8 involved hydrocarbon chains (Figure S29R). Hydrophobic benzene ring as well as carbon and nitrogen heterocycles for NOR/NOR-DPs were blocked in the middle of compounds and are not clearly presented in Figure S29J−R. Hydrophobic interactions can be enhanced by many gaps. Results revealed common potential hydrophobic interactions for NOR/NOR-DPs combined with gyrA, including hydrocarbon chains and various potential hydrophobic interactions for NOR/NOR-DPs, including piperazine rings.

Hydrogen bonds can be formed by fluorine atoms connected to hydrogen atoms (Figure S30A and Figure S30G) and cannot be formed by hydrogen bonds connected to carbon atoms (Figure S30C and Figure S30I) or benzene rings (Figure S30D, Figure S30J, Figure S30F, and Figure S30L). Hydrogen bonds can be formed by oxygen atoms connected with hydrogen atoms (Figure S30B and Figure S30H), carbon atoms (Figure S30C and Figure S30I), or benzene rings (Figure S30E, Figure S30K, Figure S30F, and Figure S30L). This phenomenon may be explained by hydrogen bond interactions that occurred after fluorine was replaced by hydroxyl groups, while the corresponding regions of NOR and other degradation products (P2, P3, P4, P5, P6, P7, and P8) exhibited no change in fluorine atoms (Figure S30 and Table S11). These results were consistent with a VDW map of the molecular surface within 4.5 Å of NOR/NOR-DPs and reveal surface properties of degradation products (Figure S29A−I). BA decreased from 350.80 $Å^2$ (NOR) to 346.21 $Å^2$ (P1), and |BE| changed from 2.53 kcal/mol (NOR) to 2.54 kcal/mol (P1), indicating that fluorine mainly affects BA (Table S7). However, the piperazine ring clearly influenced BA and |BE|.

3.5.2. Sites of Combination with NOR/NOR-DPs and GyrA. The GyrA (97 kDa) protein of *E. coli* contains 875 amino acids, the domain structure of which interacts with FQs as 571 amino acids (64 kDa) and participates in wrapping DNA as 304 amino acids (33 kDa); this protein was represented as linear blocks with proposed domain organization boundaries indicated. Key amino acid 122 in gyrA was active site tyrosine. Amino acids that led to drug resistance after mutation are numbered in italics, FQ-resistance mutations map to gyrA (83−106). Mutations at gyrA (214 and 462) confer resistance to F plasmid protein CcdB. These models were adapted from Hashimi (2019)[38] and are shown in Figure 4A. Amino acids of gyrA participated in NOR/NOR-DPS and gyrA complexing as Ile13, Glu16, Ser20, Ser27, Val28, Gly31, Asp36, Arg38, Arg46, Arg47, Tyr77, His78, His80, Asp147, Pro156, Asp157, His339, Gly340, and Gln341 (Figure 4A). The X-ray diffraction structure of gyrA and residues with high frequency (≥6) participating in NOR/NOR-DPs and gyrA combination were Ile13, Ser27, Val28, Gly31, Asp36, Arg46, Arg47, Asp157, and Gly340, of which Ile13, Ser27, Val28, Gly31, and Gly340 performance was a property of neutral amino acid, Asp36 and Asp157 performance was a property of acidic amino acid, Arg46 and Arg47 performance was a property of basic amino acid (Figure 4B−C and Table S12), percentage of neutral amino acids for high amino acids was 55.6% as highest, acidic amino acids for high amino acids was 22.2%, and basic amino acids for high amino acids was 22.2% (Table S13). Details are described in Supplementary Text S8.

When species and properties of amino acids in NOR/NOR-DPs and gyrA were compared, common neutral amino acids included Ile13 and Gly31; common acidic amino acids included Asp36; common basic amino acids included Arg47; various neutral amino acids included Ser27, Val28, and Gly340; various acidic amino acids included Asp157; and various basic amino acids included Arg46. These key amino acids could be vital sites for decreasing toxicity of NOR/NOR-DPs in future research; neutral amino acids account for a large proportion for NOR/NOR-DPs and the gyrA complex.

3.5.3. Combination Modes for Interaction with NOR/NOR-DPs and GyrA. The combination modes for NOR/NOR-DPs and gyrA combinations included hydrogen bonding and hydrophobic interactions (Table S7). There were 53 hydrogen bonds and 36 hydrophobic interactions among NOR/NOR-DPs and gyrA combinations; the percentage of hydrogen bonds for combination modes was 59.6%, while the percentage of hydrophobic interactions was 40.4% (Table S14). Nine hydrogen bonds and five hydrophobic interactions were found in NOR/NOR-DPS and Ile13 combinations, four hydrogen bonds and five hydrophobic interactions were found in NOR/NOR-DPS and Ser27 combinations, seven hydrophobic interactions were found in NOR/NOR-DPS and Val28 combinations, four hydrogen bonds and seven hydrophobic interactions were found in NOR/NOR-DPS and Gly31 combinations, nine hydrogen bonds were found in NOR/NOR-DPS and Asp36 combinations, nine hydrogen bonds were found in NOR/NOR-DPS and Arg46 combinations, nine hydrogen bonds and three hydrophobic interactions were found in NOR/NOR-DPS and Arg47 combinations, seven hydrogen bonds and three hydrophobic interactions were found in NOR/NOR-DPS and Asp157 combinations, and four hydrogen bonds and six hydrophobic interactions were found in NOR/NOR-DPs and Gly340 combinations (Table S15 and Table S16). Details are described in Supplementary Text S9.

The order of sum of hydrogen bonds between NOR/NOR-DPs and gyrA from most to least common was P6 (422.08%) > P4 (386.25%) > P1 (372.32%) > P5 (355.48%) > P7 (285.90%) > P3 (274.65%) > P8 (205.20%) > P2 (166.32%) > NOR (78.98%) (Figure 5A and Table S7). In brief, the UV/H_2O_2 process strengthened hydrogen bonds of P1, P2, P3, P4, P5, P6, P7, and P8. Compared with NOR, hydrogen bonds of NOR-DPs were increased by the changed fluorine atom for P1, broken piperazine ring for P2, P3, and P4, exposed structure of the hydroxyl group for P5 and P6, and exposed structure of the carbonyl for P7 and P8. The sum of hydrogen bonds for P6 was maximal, which could be related to second hydroxylation.

Compared with the percentage of hydrogen bonds and hydrophobic interactions, hydrogen bonds accounted for a large proportion and vital combination modes for combination with NOR/NOR-DPs and gyrA, and hydrophobic interactions were also important for combination. Common amino acids involved in hydrogen bonds for combination with NOR/NOR-DPs and gyrA were Ile13, Asp36, and Arg47; various amino acids of hydrogen bonds were Ser27, Val28, Gly31, Arg46, Asp157, and Gly340. Various amino acids involved in hydrophobic interactions for combination with NOR/NOR-DPs and gyrA were Ile13, Ser27, Val28, Gly31, Asp36, Arg46, Arg47, Asp157, and Gly340. The sum of hydrogen bonds for

https://doi.org/10.1021/envhealth.4c00095
Environ. Health 2024, 2, 886−901

P6 was maximal, and the second hydroxylation step played an important role in this effect.

3.5.4. Binding Area for Combination with NOR/NOR-DPs and GyrA. The sequence of BA values[39,40] between NOR/NOR-DPs and gyrA from strongest to weakest was as follows: P7 (362.67 Å^2) > P8 (359.35 Å^2) > P6 (353.91 Å^2) > NOR (350.80 Å^2) > P2 (349.28 Å^2) > P1 (346.21 Å^2) > P3 (340.26 Å^2) > P5 (330.39 Å^2) > P4 (263.54 Å^2) (Figure 5B and Table S7). In brief, the UV/H_2O_2 process increased BA of P6, P7, and P8 and decreased BA of P1, P2, P3, P4, and P5. Compared with NOR, BA of NOR-DPs was increased by the exposed hydroxyl group in P6, as well as the exposed carbonyl structure in P7 and P8; this value was decreased by the altered fluorine atom in P1, broken piperazine ring in P2, P3, P4, and exposed hydroxyl group in P5. BA for P7 was maximal and could be related to carbonylation. Moreover, steric hindrance of NOR/NOR-DPs plays an important role in the BA process.[41]

3.5.5. Binding Energy of NOR/NOR-DPs in Combination with GyrA. The sequence of |BE| values for NOR/NOR-DPs and gyrA from strongest to weakest was as follows: P4 (2.69 kcal/mol) > P3 (2.58 kcal/mol) > P1 (2.54 kcal/mol) > NOR (2.53 kcal/mol) > P2 (2.41 kcal/mol) > P7 (2.39 kcal/mol) > P5 (2.36 kcal/mol) > P8 (2.23 kcal/mol) > P6 (2.11 kcal/mol) (Figure 5C and Table S7). In brief, the UV/H_2O_2 process increased |BE| of P1, P3, and P4 and decreased |BE| of P2, P5, P6, P7, and P8. Compared with NOR, |BE| of NOR-DPs was increased due to the altered fluorine atom in P1 and broken piperazine ring in P3 and P4; this value was decreased by the broken piperazine ring in P2, exposed hydroxyl group in P5 and P6, and exposed carbonyl structure in P7 and P8. |BE| for P4 was maximal, which could be related to further processing of the broken piperazine ring.

3.6. Correlations of MW, BA, and |BE| for NOR/NOR-DPs and GyrA Complex

3.6.1. Correlations between MW, BA, and |BE| for NOR/NOR-DPs and GyrA. Interaction between NOR/NOR-DPs and gyrA increased with increasing BA. MW and BA contents were estimated from curve plots, with MW plotted as the abscissa and BA plotted as the ordinate, which facilitated correlation analysis between MW and BA. The sequence of BA values between NOR/NOR-DPs and gyrA from most to least common was as follows: P7 (333.31 g/mol, 362.67 Å^2) > P8 (347.30 g/mol, 359.35 Å^2) > P6 (351.33 g/mol, 353.91 Å^2) > NOR (319.33 g/mol, 350.80 Å^2) > P2 (333.31 g/mol, 349.28 Å^2) > P1 (317.34 g/mol, 346.21 Å^2) > P3 (293.29 g/mol, 340.26 Å^2) > P5 (335.33 g/mol, 330.39 Å^2) > P4 (266.23 g/mol, 263.54 Å^2) (Figure 5D, Table S1, and Table S7). In brief, there were positive correlations between the MW of NOR/NOR-DPs and BA of NOR/NOR-DPs and gyrA, and greater BA was associated with greater MW.

The interaction between NOR/NOR-DPs and gyrA increased with increasing |BE|. MW and |BE| were estimated from curve graphs, with MW plotted as the abscissa and |BE| plotted as the ordinate, facilitating correlation analysis between MW and |BE|. The sequence of |BE| values for NOR/NOR-DPs and gyrA from most to least common was as follows: P4 (266.23 g/mol, 2.69 kcal/mol) > P3 (293.29 g/mol, 2.58 kcal/mol) > P1 (317.34 g/mol, 2.54 kcal/mol) > NOR (319.33 g/mol, 2.53 kcal/mol) > P2 (333.31 g/mol, 2.41 kcal/mol) > P7 (333.31 g/mol, 2.39 kcal/mol) > P5 (335.33 g/mol, 2.36 kcal/mol) > P8 (347.30 g/mol, 2.23 kcal/mol) > P6 (351.33 g/mol, 2.11 kcal/mol) (Figure 5D, Table S1, and Table S7). In brief, there were negative correlations between MWs of NOR/NOR-DPs and |BE| of NOR/NOR-DPs and gyrA and between lower |BE| and larger MW.

In conclusion, there were positive correlations between MWs of NOR/NOR-DPs and BA of NOR/NOR-DPs and gyrA and negative correlations between MWs of NOR/NOR-DPs and |BE| of NOR/NOR-DPs and gyrA. Moreover, the MW and spatial structure are vital factors for steric hindrance.

3.6.2. Correlations between BA, |BE| for NOR/NOR-DPs and GyrA. Interaction between NOR/NOR-DPs and gyrA was increased by a larger BA or |BE|. Data of |BE| and BA were estimated by curve graphs; |BE| was plotted as the abscissa, and BA was plotted as the ordinate, which facilitated correlation analysis between |BE| and BA. The sequence of BA values for NOR/NOR-DPs and gyrA from most to least common was as follows: P7 (2.39 kcal/mol, 362.67 Å^2) > P8 (2.23 kcal/mol, 359.35 Å^2) > P6 (2.11 kcal/mol, 353.91 Å^2) > NOR (2.53 kcal/mol, 350.80 Å^2) > P2 (2.41 kcal/mol, 349.28 Å^2) > P1 (2.54 kcal/mol, 346.21 Å^2) > P3 (2.58 kcal/mol, 340.26 Å^2) > P5 (2.36 kcal/mol, 330.39 Å^2) > P4 (2.69 kcal/mol, 263.54 Å^2) (Figure 5E and Table S7). In brief, there were negative correlations between |BE| and BA of NOR/NOR-DPs and gyrA and between lower BA and larger |BE|.

3.7. Predicted Values of IC_{50}, MIC_{50}, and MBC_{50} for NOR-DPs

The values of IC_{50}, MIC_{50}, and MBC_{50} for NOR, ciprofloxacin (CIP), moxifloxacin (MOX), ofloxacin (OFL), and levofloxacin (LEV) were obtained from literature, as shown in Table S17: values of IC_{50} of NOR, CIP, MOX, OFL, and LEV were 0.30, 0.16, 2.00, 6.00, and 47.50 μg/mL, respectively; values of MIC_{50} of NOR, CIP, MOX, OFL, and LEV were 4.00, 0.50, 0.06, 2.00, and 1.00 μg/mL, respectively; and values of MBC_{50} of NOR, CIP, MOX, OFL, and LEV were 4.00, 1.00, 0.06, 2.00, and 2.00 μg/mL, respectively.[42−48] BA and |BE| data were processed by normalization, and obtained values of η_1, η_2, and $\eta_1 + \eta_2$ are shown in Table S18. IC_{50} and MW were positively correlated; IC_{50} and BA were negatively correlated; |BE|, $\eta_1 + \eta_2$, MIC_{50}, and MBC_{50} were the same. Specifically, lower IC_{50} is associated with lower MW and larger BA, |BE|, or combination of NOR/NOR-DPs and gyrA complex; MIC_{50} and MBC_{50} have the same correlation.

The primary generation eqs 1, 2, 3 were used to calculate and predict values of IC_{50}, MIC_{50}, MBC_{50} for CIP, MOX, OFL, and LEV, respectively, as follows:

$$\frac{IC_{50NOR}}{IC_{50Xi}} = \left(\frac{MW_{NOR}}{MW_{Xi}}\right)^{a1} \times \left(\frac{BA_{Xi}}{BA_{NOR}}\right)^{b1} \times \left(\frac{|BE|_{Xi}}{|BE|_{NOR}}\right)^{c1} \times \left(\frac{(\eta_1+\eta_2)_{Xi}}{(\eta_1+\eta_2)_{NOR}}\right)^{d1} \quad (1)$$

$$\frac{MIC_{50NOR}}{MIC_{50Xi}} = \left(\frac{MW_{NOR}}{MW_{Xi}}\right)^{a2} \times \left(\frac{BA_{Xi}}{BA_{NOR}}\right)^{b2} \times \left(\frac{|BE|_{Xi}}{|BE|_{NOR}}\right)^{c2} \times \left(\frac{(\eta_1+\eta_2)_{Xi}}{(\eta_1+\eta_2)_{NOR}}\right)^{d2} \quad (2)$$

https://doi.org/10.1021/envhealth.4c00095
Environ. Health 2024, 2, 886−901

$$\frac{MBC_{50NOR}}{MBC_{50Xi}} = \left(\frac{MW_{NOR}}{MW_{Xi}}\right)^{a3} \times \left(\frac{BA_{Xi}}{BA_{NOR}}\right)^{b3} \times \left(\frac{|BE|_{Xi}}{|BE|_{NOR}}\right)^{c3} \times \left(\frac{(\eta_1+\eta_2)_{Xi}}{(\eta_1+\eta_2)_{NOR}}\right)^{d3} \quad (3)$$

where i = 1−4; $X1$ represents a compound of CIP; $X2$ represents a compound of MOX; $X3$ represents a compound of OFL; $X4$ represents a compound of LEV; indices $a1$, $a2$, and $a3$ represent power of ratio for MW_{NOR} and MW_{Xi} of IC_{50}, MIC_{50}, and MBC_{50}; indices $b1$, $b2$, and $b3$ represent power of ratio for BA_{NOR} and BA_{Xi} of IC_{50}, MIC_{50}, and MBC_{50}; indices $c1$, $c2$, and $c3$ represent power of ratio for $|BE|_{NOR}$ and $|BE|_{Xi}$ of IC_{50}, MIC_{50}, and MBC_{50}; and indices $d1$, $d2$, and $d3$ represent power of ratio for $(\eta_1+\eta_2)_{NOR}$ and $(\eta_1+\eta_2)_{Xi}$ of IC_{50}, MIC_{50}, and MBC_{50}, respectively. Details are described in Supplementary Text S10.

Additionally, eqs S4, S5, and S6 were used to generate eq 4 for IC_{50}, eq 5 for MIC_{50}, and eq 6 for MBC_{50}, which were defined as "Yang ChuanXi Rules (YCX-Rules)", respectively:

$$IC_{50Xi} = IC_{50NOR} \times \left(\frac{MW_{NOR}}{MW_{Xi}}\right)^{a1'} \times \left(\frac{BA_{NOR}}{BA_{Xi}}\right)^{b1'} \times \left(\frac{|BE|_{NOR}}{|BE|_{Xi}}\right)^{c1'} \times \left(\frac{(\eta_1+\eta_2)_{Xi}}{(\eta_1+\eta_2)_{NOR}}\right)^{d1'} \quad (4)$$

$$MIC_{50Xi} = MIC_{50NOR} \times \left(\frac{MW_{NOR}}{MW_{Xi}}\right)^{a2'} \times \left(\frac{BA_{NOR}}{BA_{Xi}}\right)^{b2'} \times \left(\frac{|BE|_{NOR}}{|BE|_{Xi}}\right)^{c2'} \times \left(\frac{(\eta_1+\eta_2)_{Xi}}{(\eta_1+\eta_2)_{NOR}}\right)^{d2'} \quad (5)$$

$$MBC_{50Xi} = MBC_{50NOR} \times \left(\frac{MW_{NOR}}{MW_{Xi}}\right)^{a3'} \times \left(\frac{BA_{NOR}}{BA_{Xi}}\right)^{b3'} \times \left(\frac{|BE|_{NOR}}{|BE|_{Xi}}\right)^{c3'} \times \left(\frac{(\eta_1+\eta_2)_{Xi}}{(\eta_1+\eta_2)_{NOR}}\right)^{d3'} \quad (6)$$

Then, calculated values of $a1'$, $b1'$, $c1'$, $d1'$, $a2'$, $b2'$, $c2'$, $d2'$, $a3'$, $b3'$, $c3'$, and $d3'$ are as follows:

$$\begin{cases} a1' = 60.02 \\ b1' = 41.15 \\ c1' = 114.74 \\ d1' = 14.04 \end{cases} \begin{cases} a2' = 25.42 \\ b2' = 45.21 \\ c2' = 57.62 \\ d2' = 12.09 \end{cases} \begin{cases} a3' = 41.97 \\ b3' = 25.08 \\ c3' = 51.25 \\ d3' = 7.19 \end{cases}$$

The predicted values of IC_{50}, MIC_{50}, and MBC_{50} for CIP, MOX, OFL, and LEV by YCX-Rules equations are as follows:

$$\begin{cases} IC_{50X1} = 0.16 \\ IC_{50X2} = 2.00 \\ IC_{50X3} = 6.00 \\ IC_{50X4} = 47.50 \end{cases} \begin{cases} MIC_{50X1} = 0.50 \\ MIC_{50X2} = 0.06 \\ MIC_{50X3} = 2.00 \\ MIC_{50X4} = 1.00 \end{cases} \begin{cases} MBC_{50X1} = 1.00 \\ MBC_{50X2} = 0.06 \\ MBC_{50X3} = 2.00 \\ MBC_{50X4} = 2.00 \end{cases}$$

The predicted values of IC_{50}, MIC_{50}, and MBC_{50} for CIP ($X1$), MOX ($X2$), OFL ($X3$), and LEV ($X4$) by YCX-Rules equations were consistent with literature data.

The IC_{50}, MIC_{50}, and MBC_{50} values of NOR, MW, BA, |BE|, and $\eta_1+\eta_2$ of NOR, CIP, MOX, OFL, LEV, and NOR-DPs were used for YCX-Rules equations and applied to obtain four sets of the quaternary primary equation, respectively. Values of MW, BA, |BE|, and $\eta_1+\eta_2$ of P1−P8 used for YCX-Rules equations and obtained values of IC_{50}, MIC_{50}, MBC_{50} for P1, P2, P3, P4, P5, P6 P7, and P8 are shown in Table S19. The IC_{50} value of P4 was predicted by YCX-Rules equations; an abnormally large value may explain the lower MW and BA. The IC_{50} value of P6 was predicted by YCX-Rules, and an abnormally large value may explain the lower |BE|. The MIC_{50} value of P4 was predicted by YCX-Rules, and abnormally large values may explain the lower MW and BA values. The MBC_{50} value of P3 was predicted by YCX-Rules, and the abnormally large value may explain the lower MW. The MBC_{50} value of P4 was predicted by YCX-Rules, and the abnormally large value may explain the lower MW and BA values. Other values of IC_{50}, MIC_{50}, and MBC_{50} for NOR-DPs were within a reasonable range. This equation was used to quickly and accurately predict and calculate biotoxicity data, evaluate threats to human health, and evaluate environmental effects of NOR and other FQs in the ecological environment.

In brief, IC_{50}, MIC_{50}, and MBC_{50} values of NOR-DPs predicted by YCX-Rules equations were consistent with T.E.S.T. calculation. Compared with NOR, IC_{50} values of NOR-DPs were increased, and NOR-DPs and gyrA exhibited decreased inhibition, which is consistent with results obtained for bioaccumulation factor and oral rat LD_{50}; MIC_{50} and MBC_{50} values of NOR-DPs were between NOR and NOR-DPs, which is consistent with results obtained for developmental toxicity, *T. pyriformis* IGC_{50}, and *D. magna* LC_{50}.

4. DISCUSSION

Serious problems involving antibiotic abuse and environmental pollution worldwide have resulted from lack of awareness and management, long-term overdosage, and excessive and errant usage of antibiotics. To explore antibiotic pollution and environmental risks in water, the degradative pathway and mechanism of NOR degradation were evaluated through UV/H_2O_2 degradation technology via the LC-Q-TOF-MS system in this study. Results of NOR degradation by the LC-Q-TOF-MS system revealed fluorine-substituted products of P1 (F → ·OH), piperazine ring-cleaved products of P2 (+O−2H), P3, and P4 (−2C−H and −4C−N−6H+O, respectively), hydroxylated products of P5 and P6 (+OH and +2O2H, respectively), and carbonylated products of P7 and P8 (+O−2H and +2O−4H, respectively) of NOR via UV/H_2O_2 degradation. The UV/H_2O_2 system was constructed and applied for NOR degradation in water, and the results revealed the degradation mechanism of NOR and the production mechanism of NOR-DPs. This study could provide basic data and scientific basis for environmental risk assessment of antibiotics' pollution effect in water.

The growth inhibitory activity of NOR was detected in human cancer cell lines, including bladder carcinoma (EJ138), renal adenocarcinoma (ACHN), breast adenocarcinoma (MCF-7), hepatocyte carcinoma (HEPG2), and A549 and rat-adrenal fibroblast-pheochromocytoma (PC-12) cell lines using colorimetric MTT assay. Results showed that NOR significantly inhibited cancer cell lines and indicated that although synthesized norfloxacin tested in this study mostly acts as an antibacterial agent, it can also affect the function of type 2 DNA topoisomerase in eukaryotic cells.[49] However,

https://doi.org/10.1021/envhealth.4c00095
Environ. Health 2024, 2, 886−901

further studies are needed to elucidate the mechanisms by which NOR and its related degradation products are activated. To determine residual NOR necessary for mammalian cellular damage, cytotoxicity of NOR/NOR-DS on BV2, A549, HepG2, and Vero E6 cells was determined. Results showed that NOR/NOR-DS exhibited inconspicuous toxic effects on BV2, A549, HepG2, and Vero E6 cells: viability of BV2 cells was significantly lower (by 0.16% NOR/NOR-DS); viability of A549 cells was significantly lower (by 10.00% NOR/NOR-DS); viability of HepG2 cells was significantly lower (by 10.00% NOR/NOR-DS) without significant changes; and viability of Vero E6 cells was significantly lower (by 2.50% and 10.00% NOR/NOR-DS). To investigate the toxicity mechanism of NOR and its degradation products in mammalian cells, a method for detecting biotoxicity of NOR and NOR-DS was established. Results provided a theoretical and scientific basis for evaluating the toxicity of these pollutants and assessing their environmental risk.

With increase in computational simulation, comprehensive knowledge in chemistry, pharmacology, and biology has been applied more effectively to all stages of compound biological research and design steps, such as identifying new active molecules, optimizing physicochemical properties, assessing difficulty of synthesis, and designing synthetic routes.[50,51] Safety of the UV/H_2O_2 process for NOR degradation was evaluated, and various parameters of biotoxicity were calculated. The sequence of developmental toxicity for NOR/NOR-DPs was P8 > P7 > NOR > P2 > P5 > P1 > P3 = P4 = P6; thus, NOR and NOR-DPs had "Developmental toxicant" status. The UV/H_2O_2 process lowered the developmental toxicity of P1, P2, P3, P4, P5, and P6 and heightened the developmental toxicity of P7 and P8. The sequence of mutagenicity for NOR/NOR-DPs was P3 > P4 > P1 > P6 > P2 > P5 = P7 = P8 > NOR; NOR and NOR-DPs had "Mutagenicity positive" status. The UV/H_2O_2 process heightened the mutagenicity of P1, P2, P3, P4, P5, P6, P7, and P8. The sequence of bioaccumulation factor for NOR/NOR-DPs was NOR > P5 > P7 > P3 > P2 > P6 > P1 > P4 > P8; the UV/H_2O_2 process lowered the bioaccumulation factor of P1, P2, P3, P4, P5, P6, P7, and P8. The sequence of fathead minnow LC_{50} in 96 h for NOR/NOR-DPs was P1 = P3 = P4 = P5 = P6 = P7 = P8 > NOR = P2; NOR and NOR-DPs exhibited toxic status. The UV/H_2O_2 process did not change fathead minnow LC_{50} in 96 h of P2 and heightened fathead minnow LC_{50} in 96 h of P1, P3, P4, P5, P6, P7, and P8. The sequence of *T. pyriformis* IGC_{50} in 48 h for NOR/NOR-DPs was P1 = P5 > NOR > P3 > P4 > P2 = P7 = P8 > P6, and NOR and NOR-DPs exhibited toxic status. The UV/H_2O_2 process lowered *T. pyriformis* IGC_{50} in 48 h of P2, P3, P4, P6, P7, and P8 and heightened *T. pyriformis* IGC_{50} in 48 h of P1 and P5; the sequence of *D. magna* LC_{50} in 48 h for NOR/NOR-DPs was P3 = P4 > P2 > P1 > P7 > NOR > P5 > P8 > P6, and NOR and NOR-DPs exhibited toxic status. The UV/H_2O_2 process lowered *D. magna* LC_{50} in 48 h of P5, P6, and P8 and heightened *D. magna* LC_{50} in 48 h of P1, P2, P3, P4, and P7. The sequence of oral rat LD_{50} for NOR/NOR-DPs was NOR = P1 = P2 = P3 = P5 = P6 = P7 = P8 > P4, and NOR and NOR-DPs exhibited toxic status. The UV/H_2O_2 process lowered oral rat LD_{50} of P4 and did not change oral rat LD_{50} of P1, P2, P3, P5, P6, P7, and P8. Compared with NOR, P1−P8 presented increased mutagenicity and fathead minnow LC_{50}, decreased bioaccumulation factor and oral rat LD_{50}, and anfractuous changes in developmental toxicity, *T. pyriformis* IGC_{50}, *D. magna* LC_{50}, demonstrated by T.E.S.T. software.

Furthermore, compared with NOR, developmental toxicity of NOR-DPs was decreased due to the altered fluorine atom in P1, broken piperazine ring in P2, P3, and P4, and exposed structure of thec hydroxyl group in P5 and P6; this value was increased by the exposed structure of the carbonyl for P7 and P8; the mutagenicity of NOR-DPs was increased by the changed fluorine atom in P1, broken piperazine ring in P2, P3, and P4, exposed structure of the hydroxyl group for P5 and P6, and exposed structure of the carbonyl group for P7 and P8; the bioaccumulation factor of NOR-DPs was decreased by the changed fluorine atom for P1, broken piperazine ring for P2, P3, and P4, exposed structure of the hydroxyl group for P5 and P6, and exposed structure of the carbonyl group for P7 and P8. Fathead minnow LC_{50} in 96 h of NOR-DPs was increased by the changed fluorine atom for P1, broken piperazine ring for P3 and P4, exposed structure of the hydroxyl group for P5 and P6, and exposed structure of the carbonyl for P7 and P8; this value was decreased by the broken piperazine ring for P2. *T. pyriformis* IGC_{50} in 48 h of NOR-DPs was increased by the changed fluorine atom for P1 and exposed structure of the hydroxyl group for P5 and decreased by the broken piperazine ring for P2, P3, and P4, exposed structure of the hydroxyl group for P6, and exposed structure of the carbonyl for P7 and P8. *D. magna* LC_{50} in 48 h of NOR-DPs was increased by the changed fluorine atom for P1, broken piperazine ring for P2, P3 and P4, and exposed structure of the carbonyl for P7. This value was decreased by the exposed structure of the hydroxyl group for P5 and P6 and exposed structure of the carbonyl for P8. Oral rat LD_{50} of NOR-DPs was decreased by the changing fluorine atom for P1, broken piperazine ring for P2, P3, and P4, exposed structure of the hydroxyl group for P5 and P6, and exposed structure of the carbonyl group for P7 and P8. The UV/H_2O_2 process of piperazine ring opening, hydroxylation, and carbonylation increases biotoxicity of NOR-DPs and is vital for NOR degradation. The system for calculating the biotoxicity of NOR/NOR-DPs was established, providing a theoretical basis for calculating the biotoxicity of NOR and its degradation products.

Molecular docking software is a comprehensive application environment and technology development platform that integrates visualization, simulation, and application development in integrated software systems for pharmaceutical and life sciences.[52] The unified operating environment can fully support small-molecule compound and biological research through molecular simulation, protein structure analysis, small-molecule data processing, and protein and small-molecule docking research.[53] Common and various mechanisms of interaction, such as functional groups, amino acids with high frequency, hydrogen bonds, hydrophobic interactions, binding areas, and binding energies between NOR/NOR-DPs and gyrA, were clarified in detail by computational docking simulations. Molecular docking technology was used to investigate the molecular mechanism of inhibition between NOR-DPs and gyrA. Results of NOR/NOR-DPs showed that common functional groups of NOR and NOR-DPs include carboxyl, carbonyl, benzene ring, heterocycle of carbon and nitrogen, and hydrocarbon chain; various functional groups between NOR and NOR-DPs include fluorine, piperazine ring, hydroxyl, and nitrogen; common potential groups involved in hydrophobic interaction of NOR/NOR-DPs combined with gyrA include the hydrocarbon chain; various potential groups

https://doi.org/10.1021/envhealth.4c00095
Environ. Health 2024, 2, 886−901

involved in hydrophobic interaction of NOR/NOR-DPs include the piperazine ring. Amino acid residues of gyrA with high frequency that participated in NOR/NOR-DPs and gyrA combination were Ile13, Ser27, Val28, Gly31, Asp36, Arg46, Arg47, Asp157, and Gly340. The percentage of neutral amino acids with high frequency was 55.6%; hydrogen bonds accounted for a large proportion and vital combination modes for combination with NOR/NOR-DPs and gyrA; hydrophobic interactions were also important for combinations. Common amino acids involved in hydrogen bonds of NOR/NOR-DPs and gyrA combinations were Ile13, Asp36, and Arg47, and various amino acids involved in hydrogen bonds were Ser27, Val28, Gly31, Arg46, Asp157, and Gly340. Various amino acids involved in hydrophobic interactions for NOR/NOR-DPs and gyrA combinations were Ile13, Ser27, Val28, Gly31, Asp36, Arg46, Arg47, Asp157, and Gly340. The sum of hydrogen bonds for P6 was maximal, and second hydroxylation played an important role in this consequence. BA for P7 was maximal, which could be related to carbonylation; |BE| for P4 was maximal and could be related to a further process to a broken piperazine ring.

The common mechanism of gyrA protein and NOR/NOR-DPS complex binding was explored, and correlation analysis was performed. Correlations were evaluated as MW of NOR/NOR-DPs, BA, and |BE| for NOR/NOR-DPs and gyrA complex by the principle of QSAR theory. There were positive correlations between MW of NOR/NOR-DPs and BA of NOR/NOR-DPs and gyrA and negative correlation between MW and |BE|; moreover, there were negative correlations between |BE| and BA of NOR/NOR-DPs and gyrA and between lower BA and larger |BE|. Moreover, MW and spatial structure are vital factors for steric hindrance. A quantitative structural relationship of interaction between NOR or NOR-DPs and gyrA inhibition was constructed, which provided a basis for elucidating common mechanisms of NOR/NOR-DPs binding to gyrA and evaluating toxic effects of these proteins on the environment.

Computational simulation has been widely used because of its high efficiency, high precision, and low cost; thus, strategy is highly important for toxicology exploration and evaluation of environmental effects of NOR and other chemicals. Based on IC_{50}, MIC_{50}, and MBC_{50} values for NOR, CIP, MOX, OFL, and LEV obtained from the literature, BA and |BE| data were normalized, YCX-Rules were used to predict IC_{50}, MIC_{50}, and MBC_{50} values for NOR-DPs (P1, P2, P3, P4, P5, P6, P7, and P8). IC_{50}, MIC_{50}, and MBC_{50} data for CIP, MOX, OFL, and LEV obtained from YCX-Rules were consistent with data obtained from the literature. The reliability of YCX-Rules for predicting IC_{50}, MIC_{50}, and MBC_{50} was verified, and the authors aimed to provide a basis for toxicity prediction of other chemical substances. An optimized formula for the YCX-Rules was more suitable for calculating toxicity data of known or unknown compounds to predict biotoxicity of compounds more quickly and accurately; the formula provided a new strategy for evaluating environmental effects in toxicology.

5. CONCLUSION

NOR is a third-generation FQ antibiotic that greatly pollutes the water environment and is commonly and widely used, threatening human health and ecological system safety. Taking NOR/NOR-DPs as research objects, the toxicity of NOR results from the fluorine atom and piperazine ring. In this study, the degradation mechanism of NOR as a fluorine-substituted product (P1), piperazine ring-cleaved product (P2, P3, and P4), hydroxylated product (P5, P6), and carbonylated product (P7, P8) was explored via the UV/H_2O_2 degradation system. NOR degradation had no significant effect on the cytotoxicity of BV2, A549, HepG2, or Vero E6 cells, as determined by CCK-8 and LDH assays. In addition, mutagenicity and fathead minnow LC_{50} increased, while the bioaccumulation factor and oral rat LD_{50} decreased during the NOR degradation process, as determined by T.E.S.T. software. The molecular mechanism and structural activity relationship for inhibition of NOR/NOR-DPs and gyrA were determined by AutoDock software based on functional groups, amino acids with high frequency, hydrogen bonds of P6 (422.08%), hydrophobic interactions, BA of P7 (362.67 $Å^2$), |BE| of P4 (2.69 kcal/mol) (which was highest), and quantitative structural relationship between BA and |BE|, which had a negative correlation. The "YCX-Rules" equation was proposed to predict biotoxicity of IC_{50}, MIC_{50}, and MBC_{50} for NOR-DPs, in which MW, BA, |BE,| and sum of $\eta_1 + \eta_2$ (η_1: normalization of BA, η_2: normalization of |BE|) were considered important factors in the calculation process. These findings could provide technological support and a theoretical foundation for assessing toxic effects of NOR and other ECs in the environment and risk regulation.

■ ASSOCIATED CONTENT

Data Availability Statement

Data will be made available on request.

Supporting Information

The Supporting Information is available free of charge at https://pubs.acs.org/doi/10.1021/envhealth.4c00095.

Chemical, experimental, and theoretical process (Text S1); degradation pathways of NOR and its ESP (Text S2, Figures S1−S2); cell viability, cytotoxicity, and biotoxicity of NOR/NOR-DPs/NOR-DS (Text S3−S5, Figures S3−S6, Tables S2−S6); molecular docking between gyrA and NOR/NOR-DPs (Text S6−S9, Figures S7−S27, Tables S7−S10 and S12−S16); Yang ChuanXi Rules (Test S10, Tables S17−S19); structure and surface performance of small molecules (Figures S28−S30, Tables S1 and S11) (PDF)

■ AUTHOR INFORMATION

Corresponding Authors

Xiaoning Wang − *School of Environmental and Municipal Engineering, Qingdao University of Technology, Qingdao 266520, China*; Email: wangxn5593@163.com

Weiliang Wang − *School of Environmental and Municipal Engineering, Qingdao University of Technology, Qingdao 266520, China*; orcid.org/0000-0002-6159-1292; Email: sdqcsdnu@163.com

Authors

Chuanxi Yang − *School of Environmental and Municipal Engineering, Qingdao University of Technology, Qingdao 266520, China*; orcid.org/0000-0002-8805-5748

Xinyan Zhao − *Business School, Qingdao University of Technology, Qingdao 266520, China*

Yongkun Wu − *School of Environmental and Municipal Engineering, Qingdao University of Technology, Qingdao 266520, China*

https://doi.org/10.1021/envhealth.4c00095
Environ. Health 2024, 2, 886−901

Jingyan Lin − *School of Environmental and Municipal Engineering, Qingdao University of Technology, Qingdao 266520, China*
Yuhan Zhao − *School of Environmental and Municipal Engineering, Qingdao University of Technology, Qingdao 266520, China*
Yiyong Xu − *School of Environmental and Municipal Engineering, Qingdao University of Technology, Qingdao 266520, China*
Kaipeng Sun − *School of Environmental and Municipal Engineering, Qingdao University of Technology, Qingdao 266520, China*
Chao Zhang − *School of Environmental and Municipal Engineering, Qingdao University of Technology, Qingdao 266520, China*
Ziheng Wan − *School of Environmental and Municipal Engineering, Qingdao University of Technology, Qingdao 266520, China*
Weihua Zhao − *School of Environmental and Municipal Engineering, Qingdao University of Technology, Qingdao 266520, China*
Yihua Xiao − *School of Environmental and Municipal Engineering, Qingdao University of Technology, Qingdao 266520, China*
Haofen Sun − *School of Environmental and Municipal Engineering, Qingdao University of Technology, Qingdao 266520, China*
Dong Chen − *School of Environmental and Municipal Engineering, Qingdao University of Technology, Qingdao 266520, China*
Wenping Dong − *School of Environmental and Municipal Engineering, Qingdao University of Technology, Qingdao 266520, China*
Tieyu Wang − *Guangdong Provincial Key Laboratory of Marine Disaster Prediction and Prevention, Shantou University, Shantou 515063, China*

Complete contact information is available at: https://pubs.acs.org/10.1021/envhealth.4c00095

Author Contributions

[#]The two authors contributed equally to this work.

Author Contributions

C.X.Y., X.N.W.: Conceptualization, data curation, resources, writing−original draft. X.Y.Z, Y.K.W., J.Y.L., Y.H.Z.: Data curation, investigation. Y.Y.X., K.P.S., C.Z., Z.H.W.: Data curation, formal analysis, software. W.H.Z., Y.H.X., H.F.S., DC. W.P.D., T.Y.W., W.L.W.: Methodology, funding acquisition, supervision, writing−review and editing.

Notes

The authors declare no competing financial interest.

■ ACKNOWLEDGMENTS

This work was supported by the National Natural Science Foundation of China (41672340), Taishan Scholar Foundation of Shandong Province (tsqn201909126), and National Key Research and Development Program of China (2021YFC3201004).

■ REFERENCES

(1) Kumar, M.; Sridharan, S.; Sawarkar, A. D.; Shakeel, A.; Anerao, P.; Mannina, G.; Sharma, P.; Pandey, A. Current research trends on emerging contaminants pharmaceutical and personal care products (PPCPs): A comprehensive review. *Sci. Total Environ.* **2023**, *859*, 160031.
(2) Chen, X. X.; Fu, W. Y.; Yang, Z. C.; Yang, Y. L.; Li, Y. J.; Huang, H.; Zhang, X. H.; Pan, B. C. Enhanced H_2O_2 utilization efficiency in Fenton-like system for degradation of emerging contaminants: Oxygen vacancy-mediated activation of O_2. *Water. Res.* **2023**, *230*, 119562.
(3) Richardson, S. D.; Ternes, T. A. Water analysis: Emerging contaminants and current issues. *Anal. Chem.* **2011**, *83* (12), 4614−4648.
(4) Holmes, B.; Brogden, R. N.; Richards, D. M. Norfloxacin: A review of its antibacterial activity, pharmacokinetic properties and therapeutic use. *Drugs.* **1985**, *30*, 482−513.
(5) Du, J.; Zhao, H. X.; Liu, S. S.; Xie, H. J.; Wang, Y.; Chen, J. W. Antibiotics in the coastal water of the South Yellow Sea in China: Occurrence, distribution and ecological risks. *Sci. Total Environ.* **2017**, *595*, 521−527.
(6) Liang, X. M.; Chen, B. W.; Nie, X. P.; Shi, Z.; Huang, X. P.; Li, X. D. The distribution and partitioning of common antibiotics in water and sediment of the Pearl River Estuary, South China. *Chemosphere.* **2013**, *92* (11), 1410−1416.
(7) Zhang, R. J.; Zhang, G.; Zheng, Q.; Tang, J. H.; Chen, Y. J.; Xu, W. H.; Zou, Y. D.; Chen, X. X. Occurrence and risks of antibiotics in the Laizhou Bay, China: Impacts of river discharge. *Ecotox. Environ. Safe.* **2012**, *80*, 208−215.
(8) Li, Q. Z.; Gao, J. X.; Zhang, Q. L.; Liang, L. Z.; Tao, H. Distribution and risk assessment of antibiotics in a typical river in North China Blain. *B. Environ. Contam. Tox.* **2017**, *98* (4), 478−483.
(9) Chang, X. S.; Meyer, M. T.; Liu, X. Y.; Zhao, Q.; Chen, H.; Chen, J. A.; Qiu, Z. Q.; Yang, L.; Cao, J.; Shu, W. Q. Determination of antibiotics in sewage from hospitals, nursery and slaughter house, wastewater treatment plant and source water in Chongqing region of Three Gorge Reservoir in China. *Environ. Pollut.* **2010**, *158* (5), 1444−1450.
(10) Mohan, H.; Ramasamy, M.; Ramalingam, V.; Natesan, K.; Duraisamy, M.; Venkatachalam, J.; Shin, T.; Seralathan, K. K. Enhanced visible light-driven photocatalysis of iron-oxide/titania composite: Norfloxacin degradation mechanism and toxicity study. *J. Hazard. Mater.* **2021**, *412*, 125330.
(11) Corrado, M. L.; Struble, W. E.; Peter, C.; Hoagland, V.; Sabbaj, J. Norfloxacin: Review of safety studies. *Am. J. Med.* **1987**, *82* (6B), 22−26.
(12) Bartoskova, M.; Dobsikova, R.; Stancova, V.; Pana, O.; Zivna, D.; Plhalova, L.; Blahova, J.; Marsalek, P. Norfloxacin-toxicity for Zebrafish (Danio rerio) focused on oxidative stress parameters. *Bio. Med. Res. Int.* **2014**, *2014*, 1−6.
(13) Edwards, M. J.; Flatman, R. H.; Mitchenall, L. A.; Stevenson, C. E. M.; Le, T. B. K.; Clarke, T. A.; Mckay, A. R.; Fiedler, H. P.; Buttner, M. J.; Lawson, D. M.; Maxwell, A. A crystal structure of the bifunctional antibiotic simocyclinone D8, bound to DNA gyrase. *Science.* **2009**, *326*, 1415−1418.
(14) Yang, L.; Wold, M. S.; Li, J. J.; Kelly, T. J.; Liu, L. F. Roles of DNA topoisomerases in simian virus 40 DNA replication *in vitro*. *P. Natl. A. Sci. India. B* **1987**, *84* (4), 950−954.
(15) Cotman, A. E.; Durcik, M.; Benedetto Tiz, D.; Fulgheri, F.; Secci, D.; Sterle, M.; Možina, Š.; Skok, Ž.; Zidar, N.; Zega, A.; Ilaš, J.; Mašič, L. P.; Tomašič, T.; Hughes, D.; Huseby, D. L.; Cao, S.; Garoff, L.; Fernández, T. B.; Giachou, P.; Crone, L.; Simoff, I.; Svensson, R.; Birnir, B.; Korol, S. V.; Jin, Z.; Vicente, F.; Ramos, M. C.; de la Cruz, M.; Glinghammar, B.; Lenhammar, L.; Henderson, S. R.; Mundy, J. E. A.; Maxwell, A.; Stevenson, C. E. M.; Lawson, D. M.; Janssen, G. V.; Sterk, G. J.; Kikelj, D. Discovery and hit-to-lead optimization of benzothiazole scaffold-based DNA gyrase inhibitors with potent activity against acinetobacter baumannii and pseudomonas aeruginosa. *J. Med. Chem.* **2023**, *66* (2), 1380−1425.
(16) Khan, T.; Sankhe, K.; Suvarna, V.; Sherje, A.; Patel, K.; Dravyakar, B. DNA gyrase inhibitors: Progress and synthesis of potent

compounds as antibacterial agents. *Biomed. Pharmacother.* **2018**, *103*, 923−938.
(17) Man, R. J.; Zhang, X. P.; Yang, Y. S.; Jiang, A. Q.; Zhu, H. L. Recent progress in small molecular inhibitors of DNA gyrase. *Curr. Med. Chem.* **2021**, *28* (28), 5808−5830.
(18) Levine, C.; Hiasa, H.; Marians, K. J. DNA gyrase and topoisomerase IV: biochemical activities, physiological roles during chromosome replication, and drug sensitivities. *BBA-Gene Struct. Express.* **1998**, *1400* (1−3), 29−43.
(19) Klevan, L.; Wang, J. C. Deoxyribonucleic acidgyrase-deoxyribonucleic acid complex containing 140 base pairs of deoxyribonucleic acid and an. alpha. 2. beta. 2 protein core. *Biochemistry* **1980**, *19* (23), 5229−5234.
(20) Dighe, S. N.; Collet, T. A. Recent advances in DNA gyrase-targeted antimicrobial agents. *Eur. J. Med. Chem.* **2020**, *199*, 112326.
(21) Garg, T.; Masud, S.; Suresh, T.; Chakraborty, T. Handling bias in toxic speech detection: A survey. *ACM Comput. Surv.* **2023**, *55* (13s), 1−32.
(22) Pillai, N.; Dasgupta, A.; Sudsakorn, S.; Fretland, J.; Mavroudis, P. D. Machine learning guided early drug discovery of small molecules. *Drug. Discovery Today.* **2022**, *27* (8), 2209−2215.
(23) Govender, P.; Müller, R.; Singh, K.; Reddy, V.; Eyermann, C. J.; Fienberg, S.; Ghorpade, S. R.; Koekemoer, L.; Myrick, A.; Schnappinger, D.; Engelhart, C.; Meshanni, J.; Byl, J. A. W.; Osheroff, N.; Singh, V.; Chibale, K.; Basarab, G. S. Spiropyrimidinetrione DNA gyrase inhibitors with potent and selective antituberculosis activity. *J. Med. Chem.* **2022**, *65* (9), 6903−6925.
(24) Yang, C. X.; Wang, X. N.; Zhang, L. L.; Dong, W. P.; Yang, C.; Shi, X. F.; Fan, Y. Q.; Wang, Y.; Lv, H. J.; Wang, W. L.; Zhao, Y. Q. Investigation of kinetics and mechanism for the degradation of antibiotic norfloxacin in wastewater by UV/H_2O_2. *J. Taiwan. Inst. Chem. E* **2020**, *115*, 117−127.
(25) Kučić, N.; Rački, V.; Jurdana, K.; Marcelić, M.; Grabušić, K. Immunometabolic phenotype of BV-2 microglia cells upon murine cytomegalovirus infection. *J. Neurovirol.* **2019**, *25* (4), 496−507.
(26) Foldbjerg, R.; Dang, D. A.; Autrup, H. Cytotoxicity and genotoxicity of silver nanoparticles in the human lung cancer cell line, A549. *Arch. Toxicol.* **2011**, *85* (7), 743−750.
(27) Vincourt, V.; Escriou, V.; Largeau, C.; Bessodes, M.; Scherman, D.; Chaumeil, J. C.; Dumortier, G. Altered HepG2 cell models using etomoxir versus tert-butylhydroperoxide. *Cell. Biol. Toxicol.* **2011**, *27* (5), 363−370.
(28) Wang, X. X.; Zeng, W. W.; Osterrieder, N. Susceptibility of Vero E6 cells to tilapia lake virus (TiLV) and anti-TiLV activity of type I interferon. *Aquaculture.* **2023**, *574*, 739598.
(29) Hou, L. D.; Guan, S.; Jin, Y. R.; Sun, W. J.; Wang, Q.; Du, Y. F.; Zhang, R. Cell metabolomics to study the cytotoxicity of carbon black nanoparticles on A549 cells using UHPLC-Q/TOF-MS and multivariate data analysis. *Sci. Total Environ.* **2020**, *698*, 134122.
(30) Thounaojam, M. C.; Jadeja, R. N.; Valodkar, M.; Nagar, P. S.; Devkar, R.; Thakore, S. Oxidative stress induced apoptosis of human lung carcinoma (A549) cells by a novel copper nanorod formulation. *Food. Chem. Toxicol.* **2011**, *49* (11), 2990−2996.
(31) Du, A. F.; Fu, H. F.; Wang, P.; Zhao, C.; Wang, C. C. Enhanced catalytic peroxymonosulfate activation for sulfonamide antibiotics degradation over the supported CoSx-CuSx derived from ZIF-L(Co) immobilized on copper foam. *J. Hazard. Mater.* **2022**, *426*, 128134.
(32) Khan, T.; Sankhe, K.; Suvarna, V.; Sherje, A.; Patel, K.; Dravyakar, B. DNA gyrase inhibitors: Progress and synthesis of potent compounds as antibacterial agents. *Biomed. Pharmacother.* **2018**, *103*, 923−938.
(33) Xue, Q.; Liu, X.; Russell, P.; Li, J.; Pan, W. X.; Fu, J. J.; Zhang, A. Q. Evaluation of the binding performance of flavonoids to estrogen receptor alpha by Autodock, Autodock Vina and Surflex-Dock. *Ecotox. Environ. Safe.* **2022**, *233*, 113323.
(34) Yang, C. X.; Wang, X. N.; Ji, Y. J.; Ma, T.; Zhang, F.; Wang, Y. Q.; Ci, M. W.; Chen, D. T.; Jiang, A. X.; Wang, W. L. Photocatalytic degradation of methylene blue with ZnO@C nanocomposites: Kinetics, mechanism, and the inhibition effect on monoamine oxidase A and B. *NanoImpact.* **2019**, *15*, 100174.
(35) Wang, X. N.; Yang, C. X.; Sun, Y. Y.; Sui, X.; Zhu, T.; Wang, Q.; Wang, S.; Yang, J.; Yang, W. J.; Liu, F. Y.; Zhang, M. M.; Wang, Y. A.; Luo, Y. A novel screening strategy of anti-SARS-CoV-2 drugs *via* blocking interaction between Spike RBD and ACE2. *Environ. Int.* **2021**, *147* (7−8), 106361.
(36) Wang, X. N.; Sun, Y. Y.; Wang, Q.; Liu, F. Y.; Yang, W. J.; Sui, X.; Yang, J.; Zhang, M. M.; Wang, S.; Xiao, Z. Y.; Luo, Y.; Wang, Y. A.; Zhu, T. Potential common mechanisms of cytotoxicity induced by amide herbicides *via* TRPA1 channel activation. *Int. J. Env. Res. Pub. He.* **2022**, *19* (13), 7985.
(37) Yin, R. L.; Chen, Y. X.; He, S. X.; Li, W. B.; Zeng, L. X.; Guo, W. Q.; Zhu, M. S. *In situ* photoreduction of structural Fe(III) in a metal-organic framework for peroxydisulfate activation and efficient removal of antibiotics in real wastewater. *J. Hazard. Mater.* **2020**, *388*, 121996.
(38) Hashimi, S. M. Albicidin, a potent DNA gyrase inhibitor with clinical potential. *J. Antibiot.* **2019**, *72* (11), 785−792.
(39) DeLano, W. L.; Ultsch, M. H.; De, A. M.; Vos, N.; Wells, J. A. Convergent solutions to binding at a protein-protein interface. *Science.* **2000**, *287* (5456), 1279−1283.
(40) Wang, X. N.; Sui, X.; Sun, Y. Y.; Cui, Z. Q.; Ma, N.; Wang, S.; Yang, J.; Liu, F. Y.; Yang, W. J.; Xiao, Z. Y.; Zhu, T.; Luo, Y.; Wang, Y. A. Potential common mechanisms of cytotoxicity induced by organophosphorus pesticides *via* NLRP3 inflammasome activation. *GeoHealth.* **2024**, *8* (4), No. e2023GH000888.
(41) Mahshid, S. S.; Camiré, S.; Ricci, F.; Vallée-Bélisle, A. A highly selective electrochemical DNA-based sensor that employs steric hindrance effects to detect proteins directly in whole blood. *J. Am. Chem. Soc.* **2015**, *137* (50), 15596−15599.
(42) Gomez, C.; Ponien, P.; Serradji, N.; Lamouri, A.; Pantel, A.; Capton, E.; Jarlier, V.; Anquetin, G.; Aubry, A. Synthesis of gatifloxacin derivatives and their biological activities against *Mycobacterium leprae* and *Mycobacterium tuberculosis*. *Bioorgan. Med. Chem.* **2013**, *21* (4), 948−956.
(43) Nakatani, M.; Mizunaga, S.; Takahata, M.; Nomura, N. Inhibitory activity of garenoxacin against DNA gyrase of *Mycoplasma pneumoniae*. *J. Antimicrob. Chemoth.* **2012**, *67* (8), 1850−1852.
(44) Rifatbegović, M.; Bačić, A.; Pašić, Š.; Maksimović, Z. Antimicrobial susceptibility of *Mycoplasma bovis* isolates from Bosnia and Herzegovina. *Jpn. J. Vet. Res.* **2021**, *69* (1), 43−49.
(45) Pachanon, R.; Koide, K.; Kongsoi, S.; Nakajima, C.; Kapalamula, T. F.; Suthienkul, O.; Suzuki, Y. Interaction of the plasmid-encoded quinolone resistance protein QnrB19 with *Salmonella* Typhimurium DNA gyrase. *J. Infect. Chemother.* **2020**, *26* (11), 1139−1145.
(46) Zhao, Q. B. Effect analysis of clinical isolates of enterococci *in vitro* antibacterial. *Drug. Res.* **2015**, *24* (22), 65−66 (in Chinese).
(47) Haas, W.; Pillar, C. M.; Hesje, C. K.; Sanfilippo, C. M.; Morris, T. W. Bactericidal activity of besifloxacin against staphylococci, *Streptococcus pneumoniae* and *Haemophilus influenzae*. *J. Antimicrob. Chemoth.* **2010**, *65* (7), 1441−1447.
(48) Samra, Z.; Rosenberg, S.; Dan, M. Susceptibility of *Urea plasma urealyticum* to tetracycline, doxycycline, erythromycin, roxithromycin, clarithromycin, azithromycin, levofloxacin and moxifloxacin. *J. Chemotherapy.* **2011**, *23* (2), 77−79.
(49) Mahmoodi, M.; Foroumadi, A. R.; Rajabalian, S.; Soltani, F.; Zohoor, A. R. *In vitro* study of cytotoxic effects of new norfloxacin derivatives on human cancer cell lines. *Majallah Ulum Payah Pizishki Iran* **2006**, *8* (2), 132.
(50) Guo, R. X.; Qi, Y. M.; Li, B. B.; Tian, J.; Wang, Z. Y.; Qu, R. J. Efficient degradation of alkyl imidazole ionic liquids in simulated sunlight irradiated periodate system: Kinetics, reaction mechanisms, and toxicity evolution. *Water. Res.* **2022**, *226*, 119316.
(51) Zheng, N.; Li, N.; Lei, L.; Zhu, B. R.; Qiao, K.; Wang, Q. W.; Liang, C. Q.; Guo, Y. Y.; Yang, L. H.; Han, J.; Zhou, Y. X.; Zhou, B. S. An *in vitro* and *in vivo* study of thyroid disruption of 1,2-bis(2,4,6-

https://doi.org/10.1021/envhealth.4c00095
Environ. Health 2024, 2, 886−901

tribromophenoxy)ethane (BTBPE)-A novel brominated flame retardant. *Environ. Health.* **2024**, *2* (1), 42−51.
(52) Gu, X.; Wang, Z. X.; Wang, J.; Ouyang, W.; Wang, B. D.; Xin, M.; Lian, M. S.; Lu, S.; Lin, C. Y.; He, M. C.; Liu, X. T. Sources, trophodynamics, contamination and risk assessment of toxic metals in a coastal ecosystem by using a receptor model and Monte Carlo simulation. *J. Hazard. Mater.* **2022**, *424*, 127482.
(53) Xu, X. C. L.; Liu, Y. A.; Mo, L. Y.; Li, X. H.; Dai, J. F.; Qin, L. T. Predicting the time-dependent toxicities of binary mixtures of five antibiotics to *vibrio qinghaiensis* sp.-*Q67* based on the QSAR model. *Environ. Health.* **2024**, *2*, 465.

https://doi.org/10.1021/envhealth.4c00095
Environ. Health 2024, 2, 886−901